Morphological Attribute Profiles With Partial Reconstruction

Wenzhi Liao, *Member, IEEE*, Mauro Dalla Mura, *Member, IEEE*, Jocelyn Chanussot, *Fellow, IEEE*, Rik Bellens, *Member, IEEE*, and Wilfried Philips, *Senior Member, IEEE*

***Abstract*—Extended attribute profiles (EAPs) have been widely used for the classification of high-resolution hyperspectral images. EAPs are obtained by computing a sequence of attribute operators. Attribute filters (AFs) are connected operators, so they can modify an image by only merging its flat zones. These filters are effective when dealing with very high resolution images since they preserve the geometrical characteristics of the regions that are not removed from the image. However, AFs, being connected filters, suffer the problem of "leakage" (i.e., regions related to different structures in the image that happen to be connected by spurious links will be considered as a single object). Objects expected to disappear at a certain threshold remain present when they are connected with other objects in the image. The attributes of small objects will be mixed with their larger connected objects. In this paper, we propose a novel framework for morphological AFs with partial reconstruction and extend it to the classification of high-resolution hyperspectral images. The ultimate goal of the proposed framework is to be able to extract spatial features which better model the attributes of different objects in the remote sensed imagery, which enables better performances on classification. An important characteristic of the presented approach is that it is very robust to the ranges of rescaled principal components, as well as the selection of attribute values. Our experimental results, conducted using a variety of hyperspectral images, indicate that the proposed framework for AFs with partial reconstruction provides state-of-the-art classification results. Compared to the methods using only single EAP and stacking all EAPs computed by existing attribute opening and closing together, the proposed framework benefits significant improvements in overall classification accuracy.**

***Index Terms*—Attribute profiles (APs), classification, high spatial resolution, hyperspectral data, partial reconstruction.**

I. Introduction

RECENT advances in sensor technology have led to an increased availability of hyperspectral data at very high spatial resolution (VHR). The exploitation of spatial information (e.g., contextual relations and geometrical and structural features) plays a fundamental role in the classification of remote sensing data. A possible approach to incorporate the spatial information is the use of mathematical morphology [1]. Pesaresi and Benediktsson [1] built a morphological profile (MP) of an image by applying a sequence of opening and closing by reconstruction operators [3], using a structural element (SE) of predefined and increasing sizes. The approach in [2] extended the method in [1] for hyperspectral data with high spatial resolution. The resulting method built the MPs on the first principal components (PCs) extracted from a hyperspectral image, leading to the definition of extended MP (EMP). The approach in [4] performs spectral-based morphology using the full hyperspectral image without dimensionality reduction. In [5], kernel PCs are used to construct the EMP, with significant improvement in terms of classification accuracies compared with the conventional EMP built on PCs. Bellens *et al.* [8] proposed two MPs using both disk-shaped and linear structuring elements (SEs) to model both the width and the length of the objects in the very high resolution panchromatic urban imagery. Their method extracted the smallest size of objects by constructing MP with disk-shaped SEs and the maximum size of objects by directional profiles.

While appealing due to their efficiency to extract spatial information from VHR remote sensed imagery, the MPs have some limitations on modeling other geometrical features (e.g., textures, etc.), as well as the strong constraint of the SEs to model the concepts of different characteristics of the spatial information (e.g., size, shape, homogeneity, etc.). Recently, Dalla Mura *et al.* [9] proposed morphological attribute profiles (APs) to reduce the limitations of the MPs. The APs are obtained by applying a sequence of attribute filters (AFs) to a gray-level image [9]. AFs are operators defined in the mathematical morphology framework which operate by merging connected components at different levels in the image according to some measure computed on the components (i.e., attributes) [3]. The APs can be used to extract features that are related not only to the scale of the regions in the image but also to any measures (e.g., geometrical, textural, and spectral) that can be computed on the regions. In [10], the APs [9] were applied to the first PCs extracted from a hyperspectral image, generating an extended AP (EAP). The approach in [11] improved the classification results by constructing the EAP with the independent component analysis. Pedergnana *et al.* [12] fused morphological APs [10] computed on both hyperspectral (HS) and LiDAR data for a classification task. Pedergnana *et al.* [13] proposed a novel iterative technique based on genetic algorithms

Manuscript received July 4, 2015; revised September 4, 2015; accepted October 5, 2015. This work was supported in part by the Fund for Strategic Basic Research supported by the Agency for Innovation by Science and Technology in Flanders (SBO-IWT) project Chameleon: Domain-specific Hyperspectral Imaging Systems for Relevant Industrial Applications and in part by the Fund for Scientific Research in Flanders (FWO) project G037115N "Data fusion for image analysis in remote sensing."

W. Liao, R. Bellens, and W. Philips are with the Department of Telecommunications and Information Processing, Ghent University, 9000 Ghent, Belgium (e-mail: wenzhi.liao@telin.ugent.be; Rik.Bellens@telin.ugent.be; philips@telin.ugent.be).

M. Dalla Mura and J. Chanussot are with the Grenoble Images Parole Signal Automatique (GIPSA) Laboratory, Grenoble Institute of Technology, 38031 Grenoble, France (e-mail: mauro.dalla-mura@gipsa-lab.grenoble-inp.fr; jocelyn.chanussot@gipsa-lab.grenoble-inp.fr).

Color versions of one or more of the figures in this paper are available online at http://ieeexplore.ieee.org.

Digital Object Identifier 10.1109/TGRS.2015.2488280

to automatically optimize the selection of the optimal features from the APs. Ghamisi *et al.* [14] presented an automatic spectral–spatial classification framework for an HS image based on morphological APs and supervised feature extraction. The approach in [15] exploited sparse representations of morphological APs for HS image classification. Li *et al.* [16] developed a new framework for the classification of hyperspectral scenes combining multiple features, where EAPs were applied to model the spatial information of HS images.

However, being connected filters, AFs [18], [30] together with operators based on geodesic reconstruction [3], suffer the problem of "leakage" [19] (i.e., regions related to different semantic objects in the image that happen to be connected by spurious links will be considered as a single region), which was also referred to as "overreconstruction" problems in [8]. This phenomenon might lead to some unexpected results for remote sensed images. For example, objects which are expected to disappear at a certain scale remain present when using connected filters (e.g., AFs [9] and geodesic reconstruction [3]). The attributes of connected objects (e.g., buildings and roads and roads and parking lots are connected) in an image will be mixed together. For example, the pixels from a small building will not be characterized by the attribute (e.g., area) of the building itself but by the area of the largest connected object (possibly a highway). The situation will be even worse if the image is quantized on a small range of values, where many objects are connected, or for noisy images (regardless the quantization) since the noise component might make two adjacent nonconnected regions connected. Clearly, this might lead to poor classification performances. The leakage problem was also contrasted in mask-based second-generation connectivity and the AFs [18], [20], in which different connectivities were considered.

To overcome the limitation of overreconstruction in geodesic reconstruction [3], the approach in [8] proposed a partial reconstruction for morphological opening and closing and better modeled the shape and size of objects in an image. The effective performances of using morphological openings and closings by partial reconstruction to extract spatial information for classification can be found in our recent work [22]–[25].

In this paper, we propose a novel framework for morphological AFs with partial reconstruction and extend it to the classification of high-resolution hyperspectral images. The main characteristic of the proposed approach is that it can separate connected objects, thus better modeling the spatial information of objects in an image. It should be noted that the proposed approach is also very robust to quantization levels since, if the input images happen to be quantized on a small range of values, many objects will be connected, leading to poor performances in the analysis. Last but not least, the APs generated by using our proposed approach contain less redundant information because connected objects will disappear according to their scales. This makes our proposed method more robust on selecting values for different attributes and enables better performances when stacking all single attributes together.

The organization of this paper is as follows. Section II gives a brief review of the morphological opening and closing with partial reconstruction. Section III introduces morphological APs and its extension to hyperspectral images. In Section IV, we detailed our proposed framework for morphological AFs with partial reconstruction and its extension to hyperspectral images. The experimental results on real hyperspectral images are presented and discussed in Section V. Finally, the conclusions of this paper are drawn in Section VI.

II. Morphological Opening and Closing With Partial Reconstruction

Morphological operators act on the values of the pixels according to transformations that consider the neighborhood (with a given size and shape) of the pixels. The basic operators are dilation and erosion [3]. These operators are applied to an image with a set of known shapes, called the structuring elements. In the case of erosion, a pixel takes the minimum value of all the pixels in its neighborhood, defined by the SE. By contrast, dilation takes the maximum value of all the pixels in its neighborhood. Dilation and erosion are usually employed in pairs, either the dilation of an image followed by the erosion of the dilated result or the erosion of an image followed by the dilation of the eroded result. These combinations are known as opening and closing. An opening acts on bright objects compared with their surrounding, while closings act on dark objects. For example, an opening deletes (this means that the pixels in the object take on the value of their surrounding) bright objects that are smaller than the SE. By increasing the size of the SE, more and more objects are removed. We will use the term scale of an opening or closing to refer to this size. A vector containing the pixel values in openings and closings by the reconstruction of different scales is called the MP. The MPs carry information about the size and shape of the objects in the image.

Aside from deleting objects smaller than the SE, morphological openings and closings also deform the objects which are still present in the image [see Figs. 1(a) and 2(a)]; the corners of rectangular objects in Fig. 1(a) (square objects) are rounded. To preserve the shapes of objects, morphological openings and closings by reconstruction (i.e., geodesic reconstruction [6], [7]) are generally the tool of choice [27], [28]. The geodesic dilation (of size 1) of the grayscale marker image f and the mask image g is defined as

$$\delta_g^1(f) = \delta^1(f) \wedge g \tag{1}$$

where δ^1 is the elementary dilation [6] with SE of elementary size and $\wedge$ is the pointwise minimum. To perform the reconstruction by dilation $R_g(f)$ of f from g, we use the operator iteratively until stability (i.e., until no further change occurs)

$$R_g(f) = \lim_{n\to\infty} \delta_g^n(f) = \underbrace{\delta_g^1 \delta_g^1, \ldots, \delta_g^1(f)}_{\text{until stability}}. \tag{2}$$

An opening by reconstruction γ of an image f can be obtained by first performing a regular opening σ on the image f and using the result of this opening as the marker image and the original image as the mask for the reconstruction process

$$\gamma = R_f\left(\sigma(f)\right). \tag{3}$$

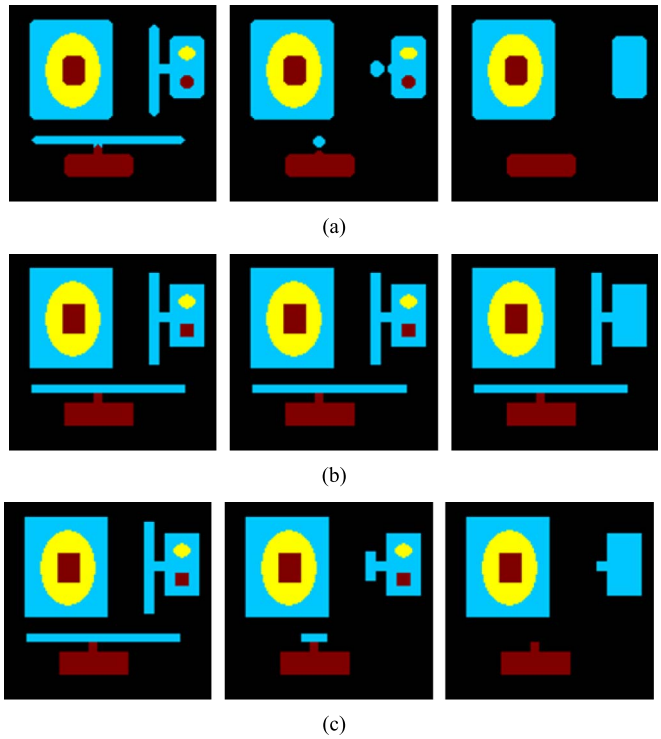

Fig. 1. Openings with disk-shaped SEs of increasing size on a synthetic image [the original image is in Fig. 3(a)]. The scales of SEs vary from 2 to 6, with steps of 2. (a) Without reconstruction. (b) Geodesic reconstruction. (c) Partial reconstruction.

Closing by reconstruction ϕ can be defined by duality (i.e., first invert the image, then perform the opening by reconstruction, and finally invert the result). We can see the results in Figs. 1(b) and 2(b); the shapes of the objects are well preserved, and some small objects disappear as the scale (here, the scale is related to the size of the SE) increases. However, an MP with reconstruction will lead to some undesirable effects (such as overreconstruction), and a lot of objects that disappeared in the MP without reconstruction remain present in the MP with reconstruction. Objects which are expected to disappear in the image at a low scale are still present at the highest scales, as shown in Fig. 1(b) (road connected with the square object on the bottom) and Fig. 2(b) (small bright road on the right).

In the geodesic reconstruction process, a pixel is reconstructed if it is connected to another pixel that was not deleted after the opening or closing. Equivalently, we can say that a pixel is reconstructed if the geodesic distance d in the mask g of that pixel is less than infinite to at least one of the pixels in the marker image f [6], [7]. The approach in [8] proposed a novel partial reconstruction, in which a pixel is reconstructed if the geodesic distance is smaller than $d < \infty$. Opening with partial reconstruction $\overline{\gamma}$ [8] is defined as follows:

$$\overline{\gamma} = \delta_f^d \left(\sigma(f)\right). \tag{4}$$

The partial reconstruction is actually the same as a geodesic dilation [6], [7] of size d. The easiest and fastest way to implement this is by doing d successive elementary geodesic dilations. This is a dilation with an elementary SE followed by an intersection with the mask. In grayscale morphology, the intersection of two images is the minimum of the two grey-scale values for each pixel. For rectangular objects with disk-shaped structuring elements, the geodesic distance d between a corner and the closest not deleted pixel equals $(\sqrt{2}-1)*R$, with R being the radius of the structuring element. Consequently, partial reconstruction with $d > (\sqrt{2}-1)*R$ completely reconstructs the corners of rectangular objects. For more details on morphological filters with partial reconstruction, we refer the reader to [8].

This way, the partial reconstruction [8] solved the problem of overreconstruction while preserving the shape of objects as much as possible and made a great improvement in the classification of remote sensing imagery [22]–[25]. As shown in Figs. 1(c) and 2(c), the shapes of objects are better preserved with partial reconstruction compared to the MP without reconstruction. However, some of the more complex shapes are not so well preserved as with geodesic reconstruction. On the other hand, many small objects which remain present in the MP with reconstruction now disappear in the case of partial reconstruction. Basically, this is because, in remote sensing (urban) scenes, different objects lie closely together, and because of noise and other effects, different objects are often connected by a sequence of pixels with similar (or more extreme) pixel values. Therefore, reconstruction considers all those connected objects as a single object, and objects will only disappear when the SE does not fit the broadest part of the connected object, even though this part might be far away from the actual object. Partial reconstruction only reconstructs the immediate surrounding of the surviving part. For more details on MP with partial reconstruction and directional MP, the readers should consult [8]. The edges of simple objects are reconstructed well, but a full retrieval of complex elongated shapes might not be obtained. For simple objects like rectangles for example, the reconstruction is complete. Since, in urban remote sensing scenes, most objects are not very complex and even rectangular shaped, partial reconstruction is very well suited.

III. Morphological APs

In this section, we will briefly review the concept of APs [9] and its extension to hyperspectral images, leading to the definition of EAP [10], [11]. APs are obtained by applying a sequence of morphological AFs to a gray-level image [9]. AFs are connected operators defined in the mathematical morphology framework which process an image by merging its connected components at different gray levels. AFs process connected components by evaluating how an attribute A compares to a given reference value λ in a binary predicate P (e.g., $P := A(C_i) > \lambda$, with C_i being the ith connected component of the upper or lower level sets of an image). If P holds true, then the region is kept unaltered; otherwise, it can be set to the grayscale value of the adjacent region with the closest gray level, thereby merging the connected components. When the region is merged to the adjacent region of a lower (greater) gray level, the operation performed is a thinning (thickening). When the criterion (e.g., area and volume associated to increasing attributes) is increasing, the attribute thinning and thickening transformations are also increasing, leading to attribute opening and attribute closing [29], respectively. For the nonincreasing criterion, we recall that different outputs of the filter are obtained according to the filtering rules that one

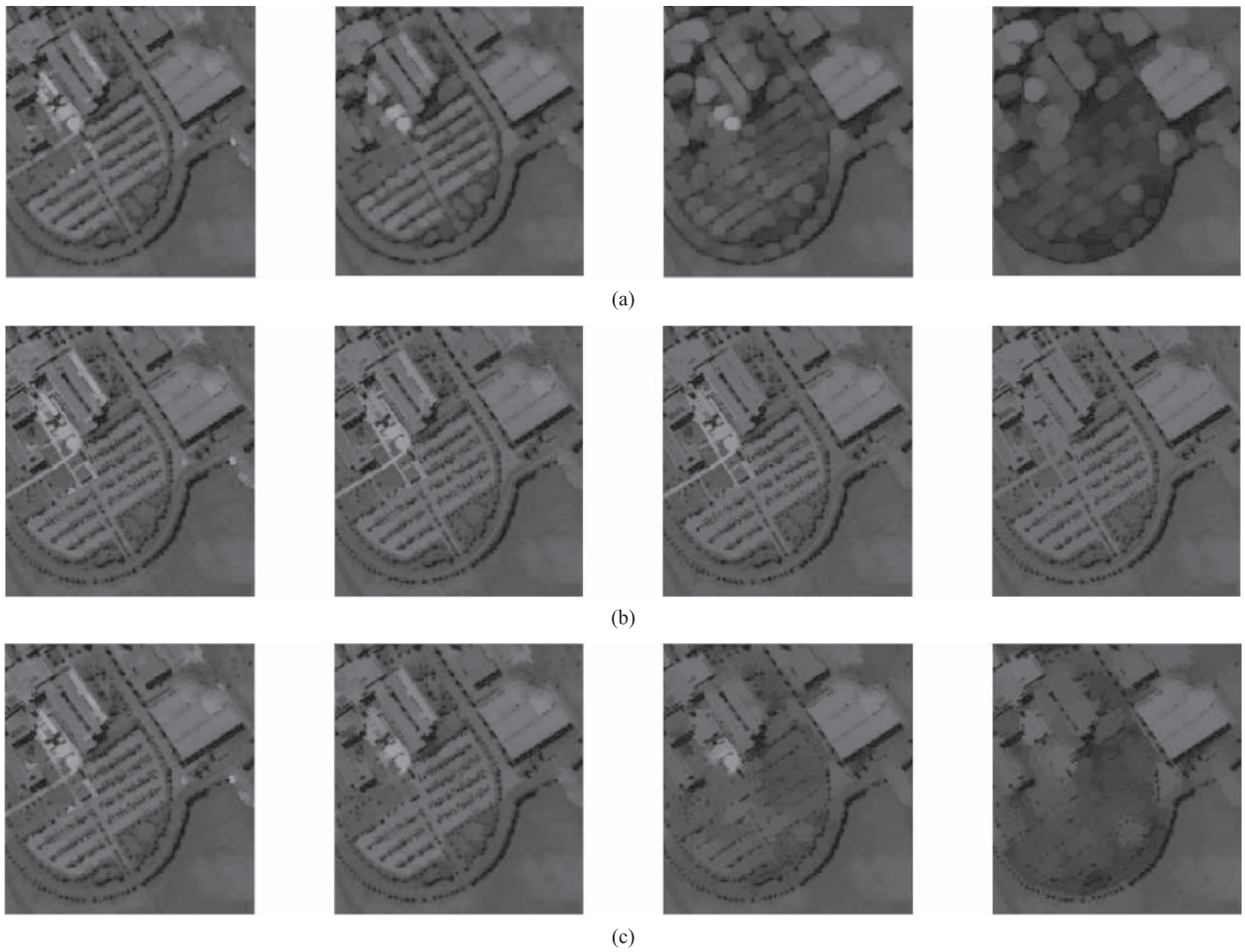

Fig. 2. Openings with disk-shaped SEs of increasing size. The scales of SEs vary from 2 to 8, with steps of 2. The image processed is part of the first PC extracted from *University Area* [see the original PC in Fig. 8(a)]. (a) Without reconstruction. (b) Geodesic reconstruction. (c) Partial reconstruction.

selects [30] because, if P holds true for a connected component, it will be merged to a darker or brighter surrounding region according to the transformation. Given a sequence of ordered criteria $\lambda = \{\lambda_1, \lambda_2, \ldots, \lambda_n\}$ (i.e., $\lambda_i <= \lambda_j$, with $i < j$), an AP is obtained by applying a sequence of attribute thinning and thickening operations to the grayscale image f

$$\mathrm{AP}(f) = \{\varphi_n(f), \ldots, \varphi_1(f), f, \rho_1(f), \ldots, \rho_n(f)\} \quad (5)$$

where φ_i and ρ_i denote the attribute thinning and thickening transformations with reference values λ_i, respectively.

EAPs [7] are an extension of APs for the analysis of hyperspectral images. Feature reduction techniques are first applied to decorrelate the hyperspectral image and extract the first m features (F_i). An EAP is obtained then by concatenating different APs computed on these m features

$$\mathrm{EAP} = \{\mathrm{AP}(F_1), \mathrm{AP}(F_2), \ldots, \mathrm{AP}(F_m)\}. \quad (6)$$

When the m EAPs obtained using different types of attributes (i.e., $\{A_1, A_2, \ldots, A_k\}$) are stacked together, the resulting profile was defined as extended multiattribute profile (MAP) (EMAP) [28]

$$\mathrm{EMAP} = \left\{\mathrm{EAP}_{A_1}, \mathrm{EAP}'_{A_2}, \ldots, \mathrm{EAP}'_{A_k}\right\} \quad (7)$$

where A_i is the ith generic attribute and $\mathrm{EAP}' = \mathrm{EAP}/\{F_1, \ldots, F_m\}$.

We recall here that, as connected operators, attribute thinning and thickening [9] operations suffer the same leakage effect. Some objects that one would expect to disappear at certain values of lambda, however, remain present after attribute filtering [see Figs. 3, 4(a), and 5(a)]. The attributes of some objects are mixed with their connected objects. This means that, in an EAP, the pixels from a small building will not be characterized by the attribute (e.g., area) of the building but by the area of the largest connected object (possibly a highway). Clearly, this might affect the classification performance.

IV. Proposed Morphological APs With Partial Reconstruction

This section details the proposed morphological AFs with partial reconstruction,[1] and its extension to hyperspectral images. Fig. 6 shows our proposed framework for morphological AFs with partial reconstruction. Our approach first uses morphological filters with partial reconstruction [8] to separate connected objects (e.g., road and parking lots) of a binary image (i.e., at one gray level) into two disjoint parts. We define two binary images to include each part of the

[1] A MATLAB application that implements the proposed morphological AFs with partial reconstruction is available on request.

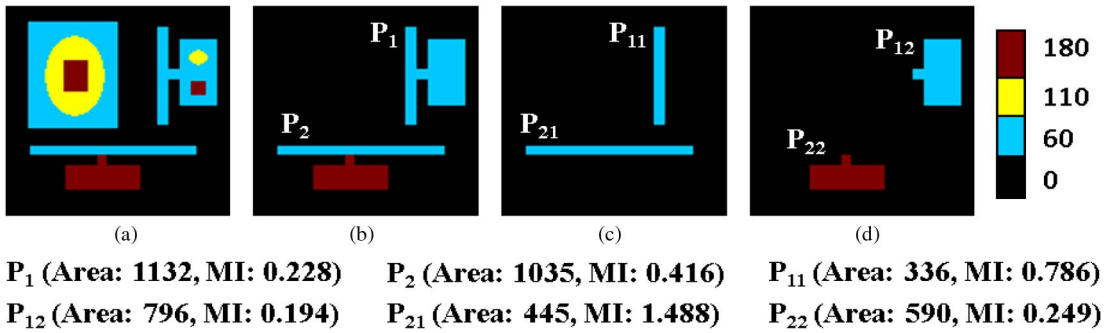

Fig. 3. Example of some connected objects and their attributes in an image. (a) Input image. (b) Connected objects with same gray level (P_1) and different gray level (P_2), and their divisions in (c) and (d).

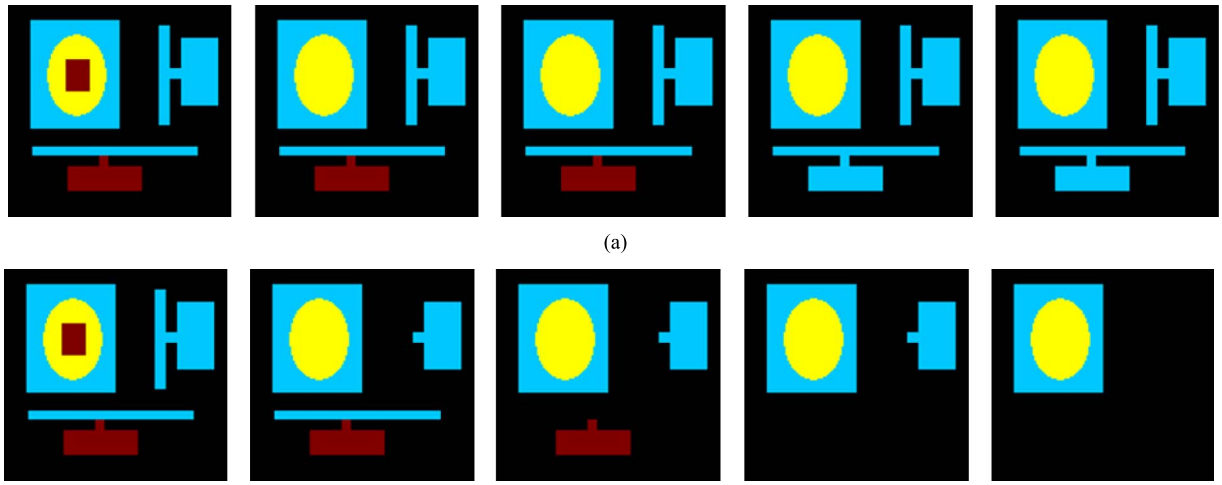

Fig. 4. Attribute thinning with "area" attribute. From left to right, the size of area was set to 200, 350, 450, 600, and 800. (a) Original attribute. (b) Proposed attribute.

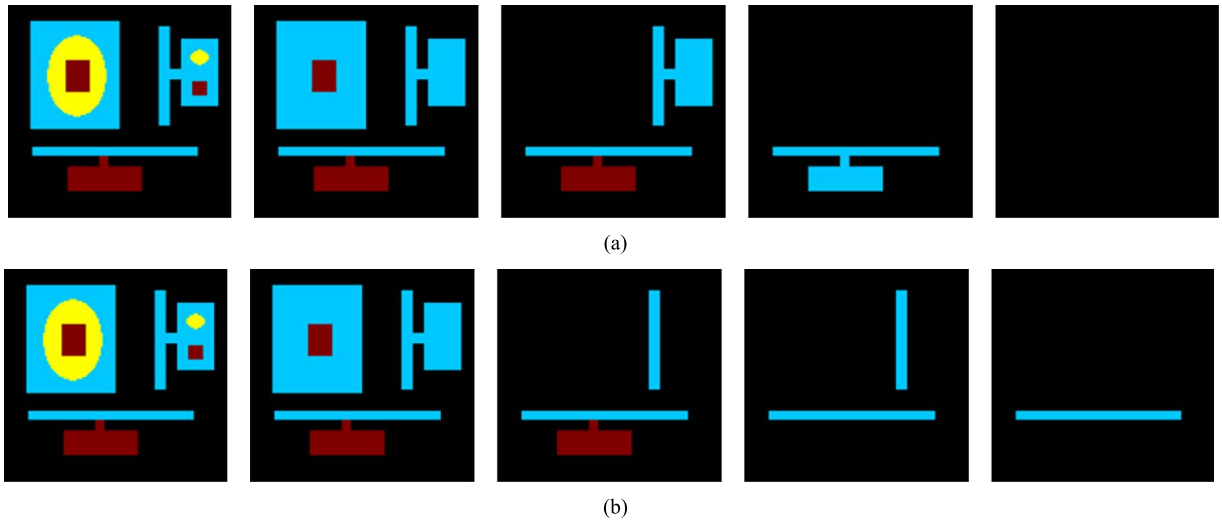

Fig. 5. Attribute thinning with "MI" attribute. From left to right, the value of MI was set to 0.15, 0.17, 0.2, 0.3, and 0.8. (a) Original attribute. (b) Proposed attribute.

separated objects. Then, we apply AFs to these two binary images. Finally, we integrate all the residuals of the filtered images and get the final output image by repeating this for all gray levels.

Suppose that f_i is the binary in gray level i [note: for opening, f_i refers to the upper level set ($f_i = f > i$), while for closing, f_i is the lower level set ($f_i = f \leq i$)]. A connected object $\mathbf{P}_k$ (kth connected component) in f_i can be separated

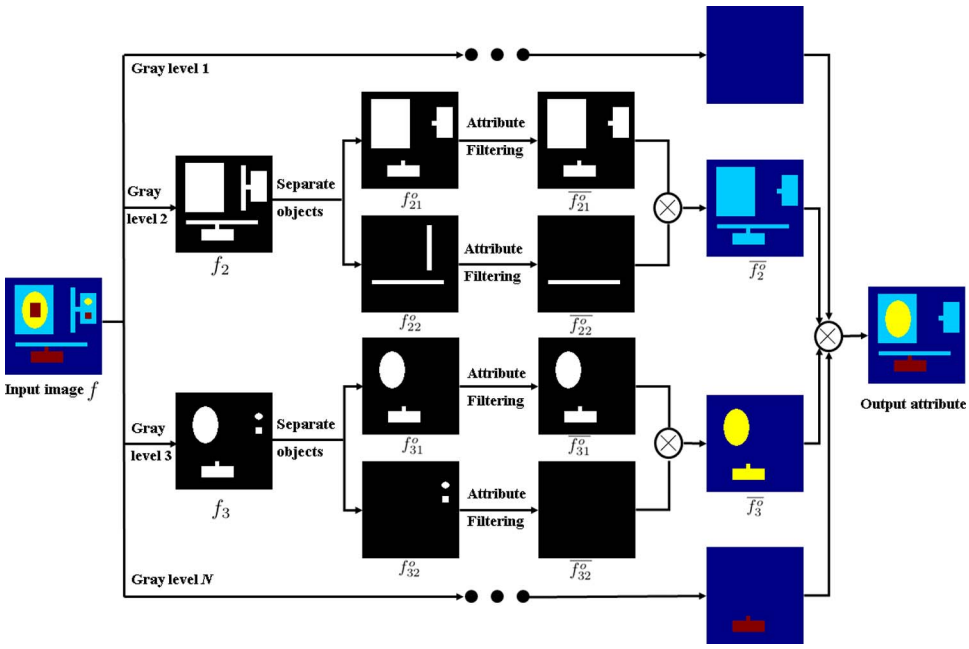

Fig. 6. Proposed framework for *attribute thinning with partial reconstruction*. Note: For opening, f_i refers to upper level set ($f_i = f > i$), while for closing, f_i is lower level set ($f_i = f \leq i$).

into two different adjacent and nonoverlapping parts $\mathbf{P}_{k1}$ and $\mathbf{P}_{k2}$ which satisfy

$$\mathbf{P}_k = \mathbf{P}_{k1} \cup \mathbf{P}_{k2} \qquad \mathbf{P}_{k1} \cap \mathbf{P}_{k2} = \emptyset. \tag{8}$$

A binary image f_i can be partitioned in its connected components (here, we refer to the foreground) $\mathbf{P}_1, \mathbf{P}_2, \ldots$, such that f_i is the union of all $\mathbf{P}_k$ and each $\mathbf{P}_k$ is a connected component, with $\mathbf{P}_k \cap \mathbf{P}_l = \emptyset$ if $k \neq l$. Let $\overline{\gamma}^j$ and $\overline{\phi}^j$ denote morphological opening and closing operators by partial reconstruction using the structuring element of size j. For opening, we first apply morphological opening with partial reconstruction in the binary image f_i (at gray level i). As the size of the SE j increases, more and more small bright objects will "disappear." We define a binary image f^o_{i1} as the filtering out at scale j, which contains one part of the connected objects $\mathbf{P}_{k1}$ in f_i as

$$f^o_{i1} = \overline{\gamma}^j(f_i). \tag{9}$$

The image which includes all "disappeared" objects of f_i, i.e., the other parts of the connected objects $\mathbf{P}_{k2}$ of f_i, can be obtained by

$$f^o_{i2} = f_i - f^o_{i1}. \tag{10}$$

Then, the two images f^c_{i1} and f^c_{i2} which contain the two disjoint parts of objects in closing can similarly be defined as

$$f^c_{i1} = \overline{\phi}^j(f_i) \tag{11}$$
$$f^c_{i2} = f_i - f^c_{i1}. \tag{12}$$

In an opening, for gray level i, we apply the binary attribute opening [29] on both binary images of f^o_{i1} and f^o_{i2} and suppose that $\overline{f^o_{i1}}$ and $\overline{f^o_{i2}}$ are their corresponding filtered-out results. We integrate the survived objects in both $\overline{f^o_{i1}}$ and $\overline{f^o_{i2}}$ into one image ($\overline{f^o_i}$) which can be formalized as

$$\overline{f^o_i} = \overline{f^o_{i1}} + \overline{f^o_{i2}}. \tag{13}$$

When repeating the binary attribute opening to the binary images $\overline{f^o_{i1}}$ and $\overline{f^o_{i2}}$ at each gray level, we define our proposed *grayscale attribute thinning with partial reconstruction* by the maximum gray level of the results of the filtering for each pixel x as

$$\overline{\rho}_\lambda(f)(x) = \max\left\{i : x \in \overline{f^o_i}\right\} \tag{14}$$

where $\lambda = \{\lambda_1, \lambda_2, \ldots, \lambda_n\}$ is a sequence of ordered criteria, same as defined in [9]. We can straightforwardly extend the definition of thinning to thickening, leading to our proposed *grayscale attribute thickening with partial reconstruction*

$$\overline{\varphi}_\lambda(f)(x) = \min\left\{i : x \in \overline{f^c_i}\right\} \tag{15}$$

where $\overline{f^c_i} = \overline{f^c_{i1}} + \overline{f^c_{i2}}$, $\overline{f^c_{i1}}$, and $\overline{f^c_{i2}}$ are the filtered-out images of f^c_{i1} and f^c_{i2} by using the binary attribute closing.

By applying a sequence of *attribute thinning and thickening with partial reconstruction* to the grayscale image f, we obtain an *AP with partial reconstruction* ($\overline{\text{AP}}$)

$$\overline{\text{AP}}(f) = \{\overline{\varphi}_n(f), \ldots, \overline{\varphi}_1(f), f, \overline{\rho}_1(f), \ldots, \overline{\rho}_n(f)\} \tag{16}$$

where $\overline{\varphi}_i$ and $\overline{\rho}_i$ denote the proposed attribute thinning and thickening with criterion λ_i, respectively.

In the original attribute thinning and thickening [9], the connected objects will survive or disappear together. As a result, different objects are considered as a single object if, in the original image, they are connected. In typical remote sensing scenes, many objects are arranged in a complex manner (similarly as simulated in Fig. 3): Roads are connected to a lot of other objects, such as parking lots (with the same gray level) and buildings (with a different gray level), etc. These individual but connected objects are often seen as a single object by the original attribute thinning and thickening [9]. For example, objects $\mathbf{P}_{11}$ and $\mathbf{P}_{21}$ in Fig. 3 are expected to disappear in the image when the sizes of the area attribute are set to 350 and 450, respectively; see Fig. 4(a). However, they remain present even when the area size is set to 800 in the original attribute thinning

and thickening [9]. While these two objects are assumed to remain with moment of inertia (MI) [9] attributes of 0.3 and 0.8, they, however, even disappear at 0.2 and 0.3, respectively, in Fig. 5(a). This means that, in an AP, the pixels from road will not be characterized by the attributes (e.g., area, MI, etc.) of the road but by the attributes of the whole connected object (and these connected objects belong to different classes). Clearly, this will lead to poor classification performances.

The proposed attribute thinning and thickening with partial reconstruction better model the spatial information of an image. The connected objects are separated and merged to a darker (opening) or brighter (closing) surrounding region according to their real attributes. By using the proposed attribute thinning and thickening with partial reconstruction, we can see objects disappear according to their real area size in Figs. 4(b) and 5(b). The algorithmic procedure of the proposed attribute thinning and thickening with partial reconstruction is formally stated in Algorithm 1.

Algorithm 1 Proposed AFs with partial reconstruction

1: Separate connected objects in the binary image f_i of gray level i into two disjoint parts by using morphological filters with partial reconstruction [8]. Note: For opening, f_i refers to upper level set ($f_i = f > i$), while for closing, f_i is lower level set ($f_i = f \leq i$). Define two binary images f_{i1}^o and f_{i2}^o as (9) and (10) to include the corresponding parts of separated objects in an opening with partial reconstruction and f_{i1}^c and f_{i2}^c as defined by (11) and (12) for a closing with partial reconstruction;
2: Apply a binary AF independently to the two binary images f_{i1}^o and f_{i2}^o (f_{i1}^c and f_{i2}^c for binary attribute closing) containing different parts of connected objects, and get their corresponding filtered-out $\overline{f_{i1}^o}$ and $\overline{f_{i2}^o}$ ($\overline{f_{i1}^c}$ and $\overline{f_{i2}^c}$ for binary attribute closing);
3: Integrate the survived objects in both $\overline{f_{i1}^o}$ and $\overline{f_{i2}^o}$ ($\overline{f_{i1}^c}$ and $\overline{f_{i2}^c}$ for binary attribute closing) into one image $\overline{f_i^o}$ ($\overline{f_i^c}$ for binary attribute closing), the same as we defined in (13);
4: Repeat 1), 2) and 3) to all gray levels, and get the results of the proposed attribute thinning and thickening with partial reconstruction by (14) and (15).

A. Extended to Hyperspectral Imagery

An AP consists of the opening profile (OP) and the closing profile (CP). For the panchromatic image, AP is built on the original single band image directly. The OP with p scales of an attribute λ_i (e.g., area) at pixel $\mathbf{x}$ forms an $n \times p$-dimensional vector, and so does the CP. Given a sequence of ordered criteria $\lambda = \{\lambda_1, \lambda_2, \ldots, \lambda_n\}$ [suppose that the filter parameter λ_i of each attribute has the same scale (e.g., p scales)], a MAP can be obtained by simply concatenating all APs in a single vector of features, with a dimensionality of $(2np + 1)$.

When applying MAPs to the hyperspectral data, feature extraction is used as a preprocessing to reduce the dimensionality of the high-dimensional original data as well as reduce the redundancy within the bands. Then, the selected features are transferred into the grayscale image by rescaling their intensities into defined ranges because the AF works on a grayscale image. An EMAP is constructed on these rescaled features. EMAP built on different features has been discussed in several studies [9], [10], [12]–[16].

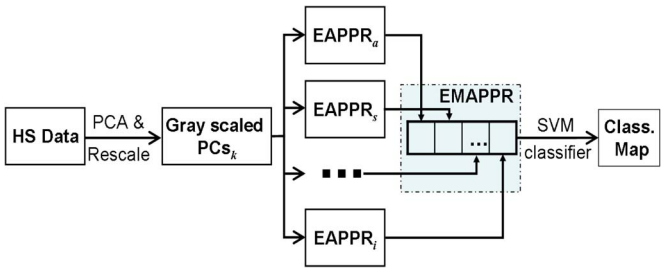

Fig. 7. Extended morphological APs with partial reconstruction for hyperspectral image.

Motivated by the construction of EMAP, we construct an EMAP with partial reconstruction (EMAPPR). The resulting method applies the proposed attribute thinning and thickening operations with partial reconstruction to construct a MAP on each rescaled feature independently. An EMAPPR is formed as a stacked vector which is constructed from all the MAPs with partial reconstruction. Supposing that m features are extracted from the original hyperspectral data to construct the EMAPPR, then the EMAPPR of pixel $\mathbf{x}$ is a $m(2np + 1)$-dimensional vector. Fig. 7 shows our framework to build EMAPPR on hyperspectral data.

When rescaling the selected features to the grayscale image, it is not easy to determine a good range of rescaled features. For high ranges, it will increase the computational time. For lower ranges, although with reduced processing time, we smooth the rescaled features, which will lead to unexpected effects (e.g., many objects will be connected). These connected objects are often treated as a single object by original attribute thinning and thickening, which consequently leads to a reduced classification performance. Figs. 8 and 9 show examples on feature with different rescaled ranges by using the original attribute thinning and the proposed attribute thinning with partial reconstruction. We can see that many small objects which should disappear at a certain scale of area attribute still remain even at a very high scale when using the original attribute thinning. This is even much worse when the selected features were rescaled to a lower range (e.g., [0, 10] in Fig. 8). This is because more objects are connected as the ranges of the rescaled features are set lower. Then, the attributes of all connected objects are mixed together, and these connected objects will remain or disappear together. In these cases, the original attribute thinning and thickening cannot well model the spatial information of objects in an image.

For another, the EMAP generated by using the original attribute thinning and thickening contains redundant information because the connected objects will survive in many scales. To test this assumption, the normalized mutual information (NMI) between each AP has been computed (see Fig. 10)

$$\mathrm{NMI}(f, g) = \frac{\mathrm{MI}(f, g)}{\sqrt{\mathrm{MI}(f, f)}\sqrt{\mathrm{MI}(g, g)}} \tag{17}$$

where the mutual information $\mathrm{MI}(f, g) = \sum_{x \in f} \sum_{y \in g} p(x, y) \log(p(x, y)/p(x)p(y))$, $p(x, y)$ is the joint probability distribution function of f and g, and $p(x)$ and $p(y)$ are the marginal

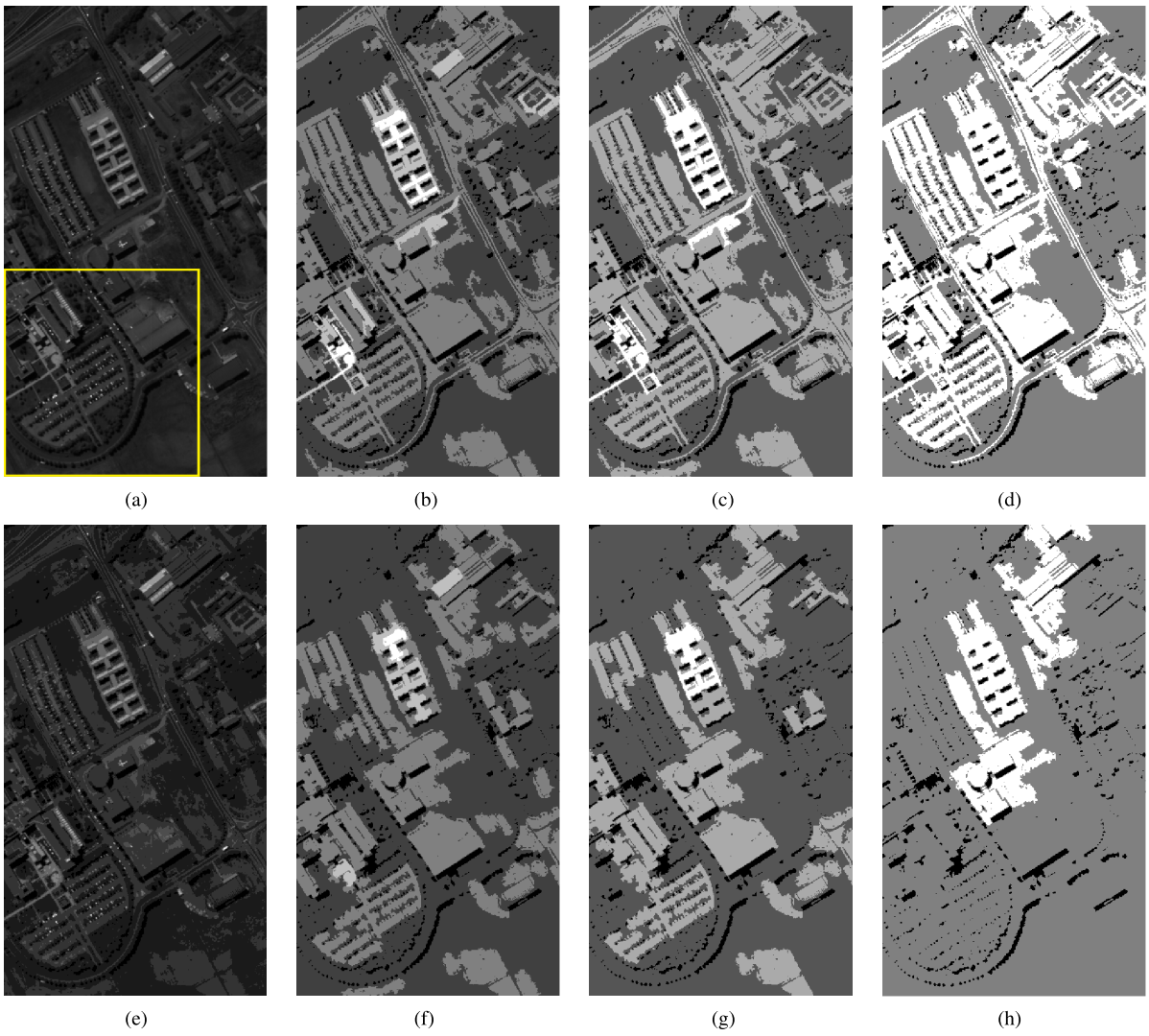

Fig. 8. Examples of "area" attribute profile computed with the first PC rescaled into range [0, 10]. The scales of area are in 500, 1000, and 5000. (a) First PC of HS image. (e) PC rescaled into range [0, 10]. (b), (c), and (d) are the AP computed by original attribute thinning. (f), (g), and (h) are the AP computed by using our proposed attribute thinning with partial reconstruction.

probability distribution functions of f and g, respectively. We apply NMI to test the independence between two variables and measure the information that the two variables share. An NMI close to 0 indicates independence, while a high NMI indicates dependence and, consequently, feature redundancy. From Fig. 10, APs generated by the proposed attribute thinning and thickening contain less redundant information than those generated by the original attribute thinning and thickening since they correspond to a lower NMI. However, some algorithms were developed to automatically select the threshold for morphological APs [26]. Recently, some artificial intelligence algorithms were used for optimal feature selection in APs [13]. However, this will increase the processing time.

The proposed attribute thinning and thickening with partial reconstruction treat the connected objects well and better model the spatial information of VHR remote sensed imagery. The connected objects are separated and merged to a darker (thinning) or brighter (thickening) surrounding region according to their real attributes. By using the proposed attribute thinning and thickening with partial reconstruction, we can see objects disappear according to their real area size in Figs. 8 and 9. Moreover, the EMAPPR generated by our proposed attribute thinning and thickening with partial reconstruction contains less redundant information. The algorithmic procedure which uses the proposed attribute thinning and thickening with partial reconstruction to build EMAPPR on an HS image for classification is formally stated in Algorithm 2.

Algorithm 2 EMAP constructed by the proposed AFs with partial reconstruction (EMAPPR)

1: Use feature extraction methods (e.g., PCA) to extract the most m significant features from the original hyperspectral data;
2: Transfer these m features into grayscale images with their intensities rescaled in a defined range;
3: Build the MAPs on each rescaled feature by using the proposed attribute thinning and thickening with partial reconstruction. Then, an EMAPPR is obtained by simply concatenating all MAPs;
4: Use the EMAPPR as an input to do classification.

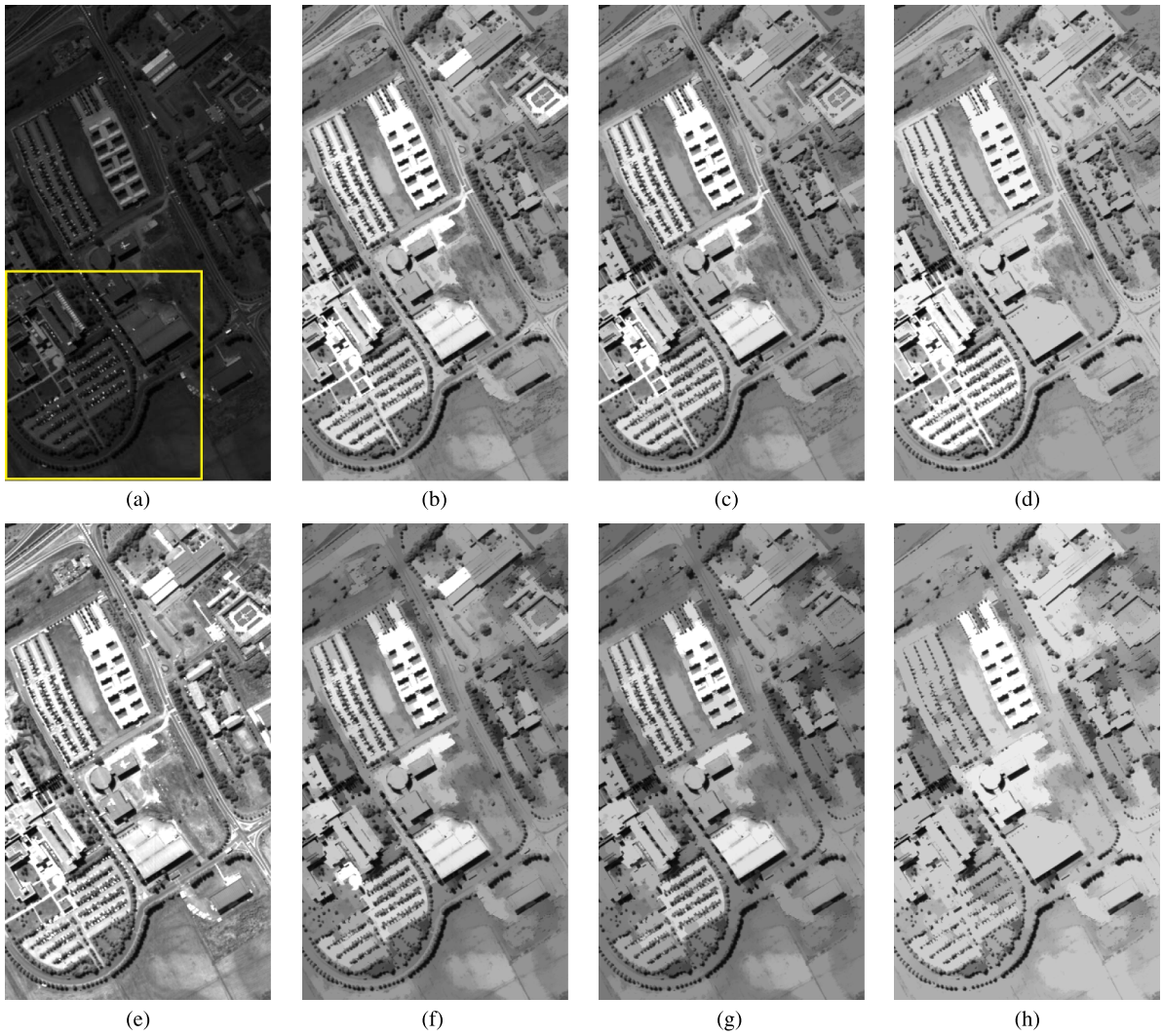

Fig. 9. Examples of "area" attribute profile computed with the first PC rescaled into range [0, 1000]. The scales of area are in 500, 1000, and 5000. (a) First PC of HS image. (e) PC rescaled into range [0, 1000]. (b), (c), and (d) are the AP computed by original attribute thinning. (f), (g), and (h) are the AP computed by using our proposed attribute thinning with partial reconstruction.

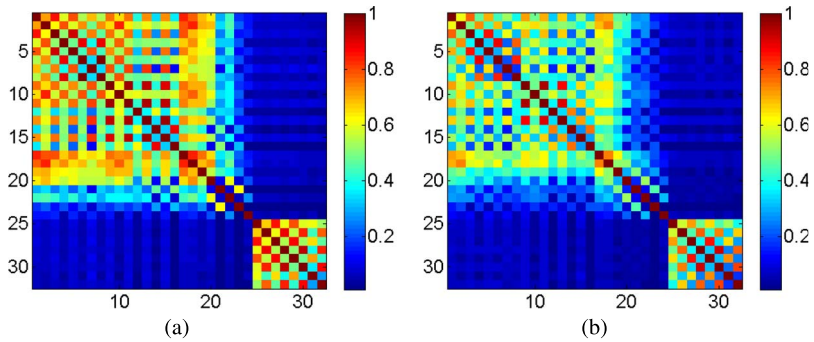

Fig. 10. Mutual information matrices for the APs of *University Area* computed on the first PC rescaled into range [0, 10]. (a) Original APs. (b) Proposed APs with partial reconstruction.

V. Experimental Results

A. Hyperspectral Image Data Sets

Experiments were run on three data sets, namely, the "*Pavia Center*," "*Pavia University*," and "*Houston University*." The first two data sets are from urban areas in the city of Pavia, Italy. The data were collected by the Reflective Optics System Imaging Spectrometer (ROSIS) sensor, with 115 spectral bands in the wavelength range from 0.43 to 0.86 μm and a very fine spatial resolution of 1.3 m by pixel.

Pavia University: The data with 610 $\times$ 340 pixels were collected over the University of Pavia, Italy. It contains 103

spectral channels after the removal of noisy bands [see Fig. 11(a) for a color composite]. The data also include nine land cover/use classes (see Table I).

Pavia Center: The data with 1096 × 492 pixels were collected over Pavia city center, Italy. It contains 102 spectral channels after the removal of noisy bands (see Fig. 12(a) for a color composite). Nine ground-truth classes were considered in experiments (see Table I). Note that the color in the cell denotes different classes in the classification maps (see Figs. 11 and 12).

Houston University: The third hyperspectral image was acquired by the National Science Foundation (NSF)-funded Center for Airborne Laser Mapping in June 2012 over the University of Houston campus and the neighboring urban area. The hyperspectral imagery has 144 spectral bands with a wavelength range from 380 to 1050 nm and with a spatial resolution of 2.5 m. The whole scene of the data, consisting of the full 349 × 1905 pixels, contains 15 classes. In our experiments, we use a subimage with a size of 349 × 1360 by removing the cloud-cover region. Available training and testing sets are given in Table V (number of training samples/number of test samples), and Fig. 13 shows the false color image of HS data and test samples. For more information, see [24] and [32].

The training and test sets for each data set (in Tables I and V) are selected pixels from the data by the experts [31], [32], corresponding to a predefined species/classes. Pixels from the training set are excluded from the test set in each case and vice versa.

B. Experimental Setup

Prior to applying the attribute thinning and thickening to hyperspectral images, principal component analysis (PCA) was first applied to the original hyperspectral data set, and the first few PCs (the first four PCs for both *Pavia Center* and *University Area* and the first two PCs for *Houston University*) were selected (representing 99% of the cumulative variance) to construct the EAPs. We used a support vector machine (SVM) [33] classifier, as it performs well even with a limited number of training samples, limiting the Hughes phenomenon [35]. The SVM classifier with radial basis function (RBF) kernels in Matlab SVM Toolbox, LIBSVM [34], is applied in our experiments. SVM with RBF kernels has two parameters: the penalty factor C and the RBF kernel widths γ. We apply a grid search on C and γ using fivefold cross-validation to find the best C within the given set $\{10^{-1}, 10^{0}, 10^{1}, 10^{2}, 10^{3}\}$ and the best γ within the given set $\{10^{-3}, 10^{-2}, 10^{-1}, 10^{0}, 10^{1}\}$. Three EAPs were computed by considering three different attributes on rescaled PCs: 1) a, area of the regions; 2) s, standard deviation (Std) of the gray-level values of the pixels in the regions; and 3) i, first moment invariant of Hu, MI. The area extracts information on the scale of the objects. The standard deviation and the MI are not dependent on the size dimension, but they are related to the geometry of the objects and the homogeneity of the intensity values of the pixels, respectively. We compare each single existing AP (EAP_a, EAP_s, and EAP_i) with our proposed AP with partial reconstruction (EAPPR_a, EAPPR_s, and EAPPR_i). We also compare the performances of stacking all EAPs or EAPPRs together, which are defined as EMAP and EMAPPR.

The classification results are quantitatively evaluated by measuring the overall accuracy (OA), the average accuracy (AA), and the Kappa coefficient (κ) on the test samples. Furthermore, the statistical significance of differences was computed using McNemar's test, which is based upon the standardized normal test statistic [36]

$$Z = \frac{f_{12} - f_{21}}{\sqrt{f_{12} + f_{21}}}$$

where f_{12} indicates the number of samples correctly by classifier 1 and incorrectly by classifier 2. The difference in accuracy between classifiers 1 and 2 is said to be statistically significant if $|Z| > 1.96$. The sign of Z indicates whether classifier 1 is more accurate than classifier 2 ($Z > 0$) or vice versa ($Z < 0$). The experiments were carried out on a 64-b 2.64-GHz Intel Xeon (1 core) CPU computer with 32-GB memory. The elapsed time includes both AP generation and classification.

C. Fair Comparisons With the Existing APs [10] on Both Pavia University and Pavia Center Data Sets

In this experiment, we make fair comparisons with the existing APs [10] on both *Pavia University* and *Pavia Center* data sets. We set the following parameters (e.g., the range of the rescaled PCs, the values of different attributes, and the training sample size) similarly as what Dalla Mura *et al.* have done in [10]. The selected PCs were rescaled to the range [0, 1000] and converted to integer in order to be processed by the AFs. Three EAPs with their values $\lambda_a = [100, 500, 1000, 5000]$, $\lambda_s = [20, 30, 40, 50]$, and $\lambda_i = [0.2, 0.3, 0.4, 0.5]$ were computed on rescaled PCs. We compared the classification performances on each single AP (EAPs and proposed EAPPRs) and all stacked APs (EMAP and our proposed EMAPPR). All the samples of the training set were used for the *Pavia University* data set, the resulting accuracies are reported in Table II, and the classification maps are shown in Fig. 11. For the *Pavia Center* data sets, only 50 samples per class were randomly selected from the full training set to train SVM classifiers, and all results were evaluated against the test set. After repeating the selection of training samples and the classification process five times, we report the mean classification results in Table III. Fig. 12 shows the best results (in terms of OA) of each method. The scene of *Pavia Center* is a very dense urban area in the center of Pavia City. Results in Table III show that only using a single attribute can provide very high classification accuracy. The APs generated by original AFs produce similar accuracies as the proposed APs. Therefore, we report the Z tests for *Pavia Center* in Table IV. From the tables and figure, we have the following findings.

1) The results confirm that including the spatial information extracted by the existing EAPs or our proposed EAPPRs in the analysis resulted in higher accuracies (up to 15% of OA) than those obtained by considering only the spectral information. In particular, for the *Pavia University* data set, the EMAPPR generated by our proposed attribute thinning and thickening with partial reconstruction produced the best results, with 15.5%–22.36% OA improvements over only using spectral features (raw and PCs), with 1.44%–17.37% OA improvements over using a single attribute (e.g., area, Std, or MI), and with 5.86% OA improvements over the EMAP generated by using the

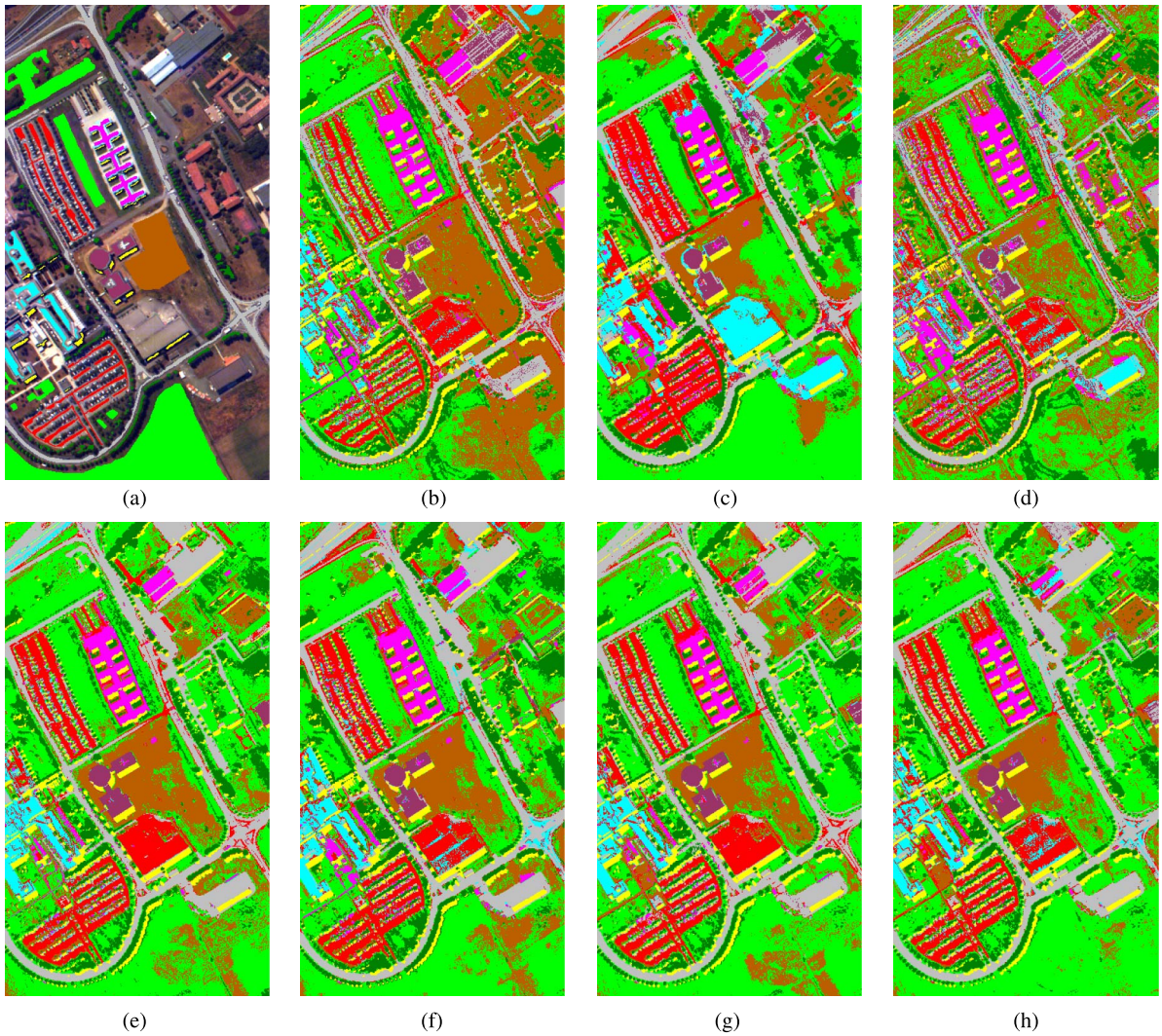

Fig. 11. Classification maps for *University Area* when the first four PCs are rescaled into range [0, 1000]. (a) RGB composition with nine classes labeled and highlighted in the image. Thematic maps using (b) morphological profile with partial reconstruction (MPPR), (c) original HS image, (d) rescaled PCs, (e) EAP_a, (f) proposed EAPPR_a, (g) EMAP, and (h) proposed EMAPPR.

TABLE I
TRAINING AND TEST SAMPLES FOR "*Pavia Center*" AND "*Pavia University*"

Pavia Center			University Area		
Class Name	# Training set	# Test set	Class Name	# Training set	# Test set
Water	745	65278	Asphalt	548	6641
Trees	785	6508	Meadows	540	18649
Meadows	797	2905	Gravel	392	2099
Bricks	485	2140	Trees	524	3064
Soil	820	6549	Metal Sheets	265	1345
Asphalt	678	7585	Soil	532	5029
Bitumen	808	7287	Bitumen	375	1330
Tiles	223	3122	Bricks	514	3682
Shadows	195	2165	Shadows	231	947

original attribute thinning and thickening [10]. For *Pavia Center*, the EMAPPR generated by our proposed attribute thinning and thickening with partial reconstruction produced the best average accuracies on OA, AA, and κ with relative lower standard deviation and leads to a significant increase of the classification accuracies, $Z > 1.96$ (see the last row in Table IV) compared to the others.

2) When considering the contribution of the single AP, the EAP_a and EAPPR_a built with the area attribute performed best in both the original APs and proposed APs. For each single AP, the EAPPRs constructed by the proposed attribute thinning and thickening with partial reconstruction perform better than the EAPs constructed by the existing attribute thinning and thickening. For *Pavia*

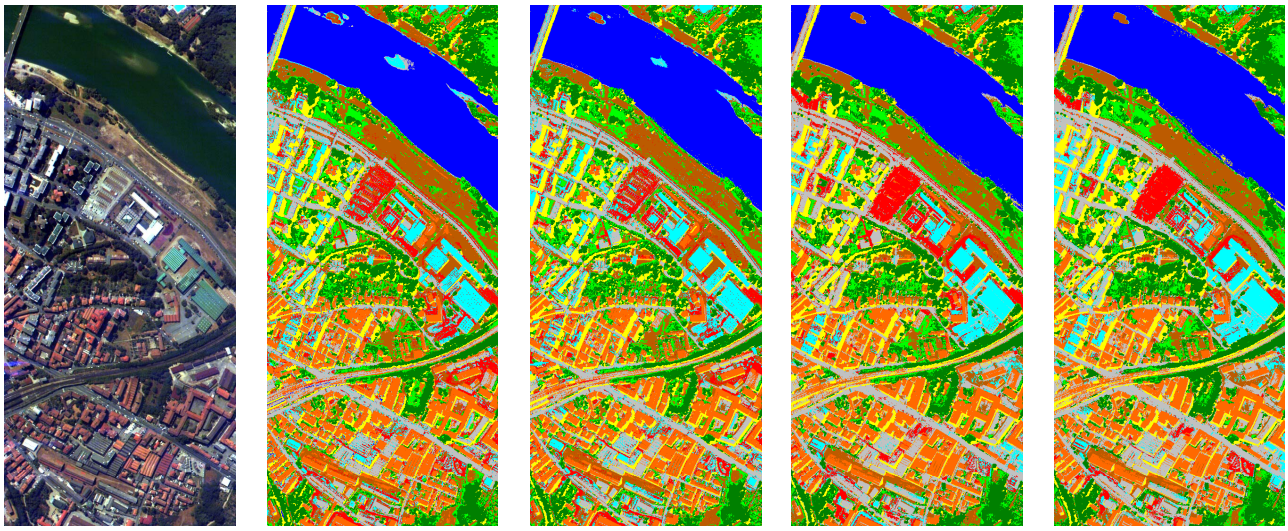

(a) (b) (c) (d) (e)

Fig. 12. Classification maps for *Pavia Center* when the first four PCs are rescaled into range [0, 1000]. (a) False color image. Thematic maps using (b) original HS image, (c) rescaled PCs, (d) EMAP, and (e) proposed EMAPPR.

University, the improvements of the proposed EAPPRs over EAPs are 2.52%, 1.38%, and 4.7% for area, Std, and MI attributes, respectively. For *Pavia Center*, the differences between the classification using the proposed EAPPRs and EAPs to build "area" and "MI" attributes are statistically significant, with $Z > 1.96$. The difference of the "Std" attribute between using the proposed EAPPRs and the existing EAPs is not statistically significant, as $Z = 0.48$ which is smaller than 1.96. When using the EAPs, it is better sometimes to use single EAPs than simply stacking many of them for classification. By simply stacking all single AP s together to form an EMAP, the OA drops almost by 2% compared to the single area attribute in *Pavia University*.

The hyperspectral remote sensing data from the urban area were a mix between man-made structures and natural materials. Many objects are made of the same material (e.g., roofs and roads made with the same asphalt), so only using single spectral features is not enough for a reliable classification. The effect of object connecting is not so obvious when rescaling the selected PCs into a larger range [see the Fig. 11(d)]. However, the EMAP generated by using original attribute thinning and thickening contains redundant information because some connected objects will survive in many scales (see the top row in Fig. 8). That is why EMAP sometimes performs even worse than single EAPs, and this will be much worse when the selected PCs are rescaled into the lower range (we will discuss this in the following section).

D. Results on Houston University

In this experiment, we apply the existing APs and our proposed APs with partial reconstruction to a new data set. The selected PCs were rescaled to the range [0, 100] and converted to integer in order to be processed by the AFs. Three EAPs with their values $\lambda_a = [100, 500, 1000, 2000, 3000, 4000, 5000]$, $\lambda_s = [0.5, 1, 2, 3, 4, 5, 6]$, and $\lambda_i = [0.15, 0.2, 0.25, 0.3, 0.35, 0.4, 0.45]$ were computed on rescaled PCs. After computing the classification performances on each single AP (EAPs and EAPPRs) and stacking all APs together (EMAP and EMAPPR), we report the resulting accuracies and the Z tests in Tables V and VI and show the classification maps in Fig. 13. This data set is very challenging for classification since the spectral and the spatial information are very similar in some man-made objects (e.g., "Residential" and "Commercial," "Road" and "Highway," and "Parking Lot 1" and "Parking Lot 1"). Results show that only using the spectral information can provide high classification accuracy (with OA up to 92%) because very limited ground truth is available for validation. Some objects are obviously misclassified [see Fig. 13(c)]; "Roads" are misclassified into "Railway." Including the spatial information extracted by the EAPPRs in the analysis resulted in almost 3% improvements in OA over those obtained by considering only the spectral information. In particular, the proposed EMAPPR produced the best results on OA, AA, and κ and leads to a significant increase of the classification accuracies, with $Z > 1.96$ (see the last row in Table VI), with 2.64%–15.27% OA improvements over only using spectral features (raw and PCs), with 1.9%–8.84% OA improvements over using a single attribute (e.g., area, Std, or MI), and with 2.28% OA improvements over the EMAP generated by using the existing attribute thinning and thickening [10].

For the classification performances of using the single EAP, the area attribute performed the best in both EAPs and proposed EAPPRs. For each single AP, the EAPPRs perform better than EAPs. The improvements of using the proposed EAPPRs over using EAPs are almost 2% for the area, Std, and MI attributes, respectively. Moreover, the differences between the classification using the proposed attribute thinning and thickening with partial reconstruction and the existing attribute thinning and thickening to build "area," "Std," and "MI" attributes are statistically significant, with $Z > 1.96$. The improvements of EMAP over raw data are not statistically significant because $Z = 1.23$, which is lower than 1.96. Even using single

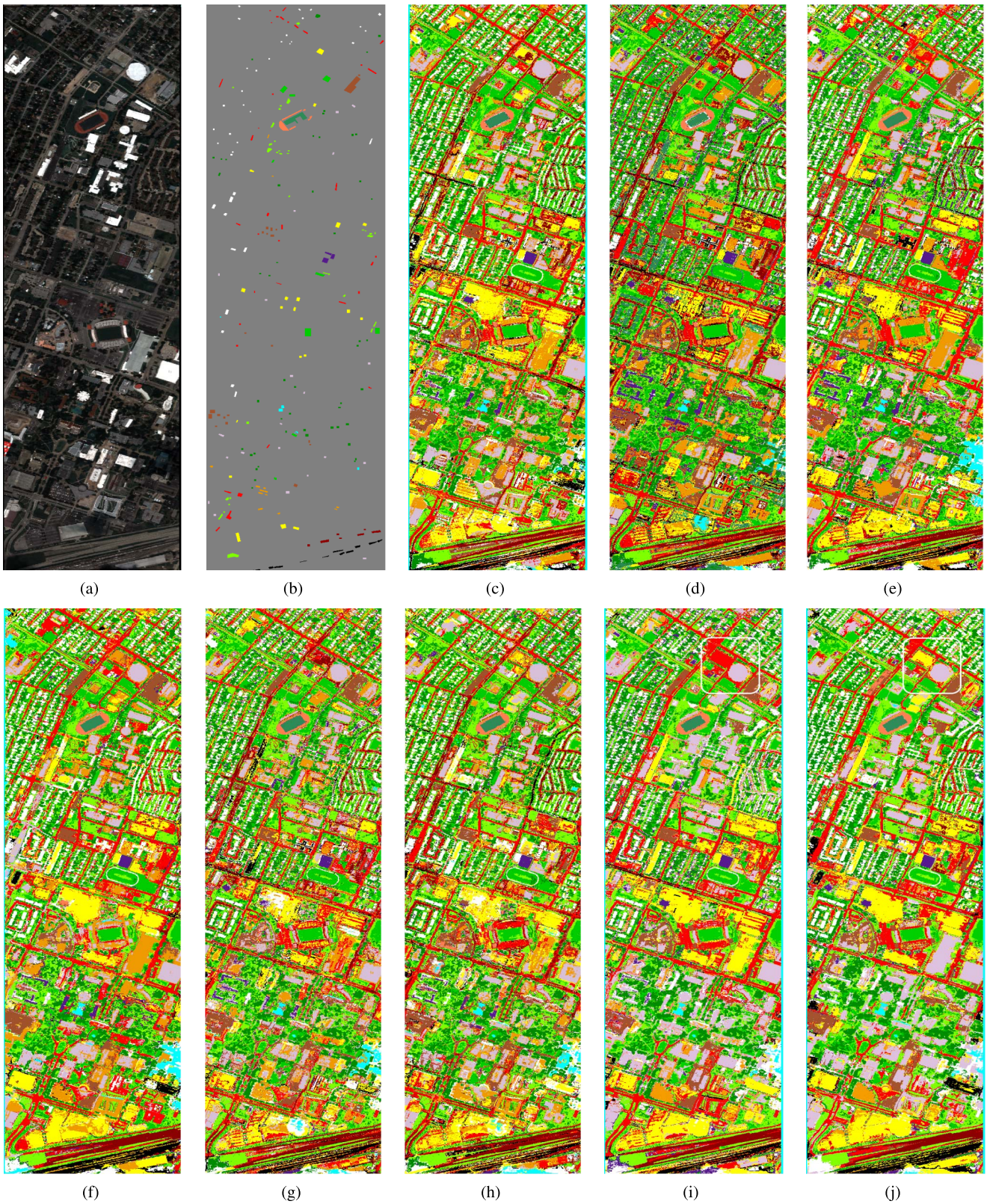

Fig. 13. Classification maps for *University Houston* when the first few PCs are rescaled into range [0, 100]. (a) False color image. (b) Ground truth. Thematic maps using (c) Original HS image. (d) Rescaled PCs. (e) EAP_s. (f) Proposed EAPPR_s. (g) EAP_i. (h) Proposed EAPPR_i. (i) EMAP, and (j) Proposed EMAPPR.

EAPPR_a, we have significant improvement over raw data, with $Z = 2.8$, which is higher than 1.96. From the classification maps, we can see visually that the connected objects are better classified by using our proposed APs with partial reconstruction because the spatial information is better modeled by our proposed method.

TABLE II
University Area: CLASSIFICATION ACCURACIES OBTAINED BY ORIGINAL APS AND OUR PROPOSED APS WITH PARTIAL RECONSTRUCTION. THE FIRST FOUR PCS ARE ALL RESCALED INTO RANGE [0, 1000]. MPPR (MORPHOLOGICAL PROFILE WITH PARTIAL RECONSTRUCTION)

	Raw	PCs	MPPR	Original attribute profiles				Proposed attribute profiles			
				EAP_a	EAP_s	EAP_i	EMAP	$EAPPR_a$	$EAPPR_s$	$EAPPR_i$	EMAPPR
No. Fea	102	4	36	36	36	36	108	36	36	36	108
OA	79.74	72.88	90.50	91.28	87.96	77.87	89.38	93.8	89.34	82.57	**95.24**
AA	88.26	82.05	89.10	93.79	90.17	82.72	92.67	**95.88**	91.19	87.74	94.99
κ	74.68	66.16	87.21	88.65	84.31	71.42	86.21	91.87	85.99	77.52	**93.66**
Asphalt	84.17	72.30	87.02	**95.97**	85.06	88.33	95.51	93.30	89.53	89.26	95.33
Meadows	67.40	63.29	98.53	87.66	88.05	74.92	84.85	92.55	89.79	78.18	**98.03**
Gravel	73.65	58.79	70.46	74.99	77.70	59.65	72.22	**93.57**	83.09	70.46	84.28
Trees	94.78	94.91	95.95	96.87	89.49	90.57	**97.16**	96.38	89.85	93.41	96.74
Metal Sheets	99.63	**99.93**	99.93	**99.93**	99.70	99.70	**99.93**	99.85	**99.93**	99.77	**99.93**
Soil	**92.32**	74.47	60.05	90.40	88.84	58.32	86.44	91.85	80.39	69.18	83.52
Bitumen	91.20	87.89	91.88	**99.92**	97.37	90.98	99.77	99.68	94.66	96.24	99.77
Bricks	91.47	87.97	98.29	**98.51**	85.31	82.08	98.23	95.84	93.51	93.35	97.45
Shadows	99.68	98.94	99.79	99.89	**100.0**	99.89	99.89	99.89	**100.0**	99.79	99.89

TABLE III
Pavia Center: CLASSIFICATION ACCURACIES OBTAINED BY ORIGINAL APS AND OUR PROPOSED APS WITH PARTIAL RECONSTRUCTION. THE FIRST FOUR PCS ARE ALL RESCALED INTO RANGE [0, 1000]

	Raw	PCs	MPPR	Original attribute profiles				Proposed attribute profiles			
				EAP_a	EAP_s	EAP_i	EMAP	$EAPPR_a$	$EAPPR_s$	$EAPPR_i$	EMAPPR
No. Fea	102	4	36	36	36	36	108	36	36	36	108
OA	94.90	95.66		98.26	98.26	94.04	98.47	98.58	98.40	94.82	**98.71**
AA	92.48	91.54		96.82	96.46	91.85	97.03	97.40	96.78	91.88	**97.54**
κ	0.914	0.926		0.970	0.970	0.900	0.974	0.976	0.973	0.913	**0.978**
Std	0.94	1.05		0.24	0.26	1.01	0.14	**0.04**	0.16	1.02	0.15

TABLE IV
Pavia Center: STATISTICAL SIGNIFICANCE OF DIFFERENCES IN CLASSIFICATION (Z) WHEN THE FIRST FEW PCS ARE RESCALED INTO RANGE [0, 1000]. EACH CASE OF THE TABLE REPRESENTS Z_{rc} WHERE r IS THE ROW AND c IS THE COLUMN

Z_{rc}		Raw	PCs	Original attributes				Proposed attributes			
				EAP_a	EAP_s	EAP_i	EMAP	$EAPPR_a$	$EAPPR_s$	$EAPPR_i$	EMAPPR
Raw		0	8.81	-42.84	-42.99	12.53	-42.73	-43.28	-42.92	-0.58	-47.91
PCs		-8.81	0	-39.36	-38.82	19.84	-38.90	-40.15	-38.47	5.97	-44.24
Original attributes	EAP_a	42.84	39.36	0	-1.21	52.22	-2.53	-3.98	-1.56	40.60	-10.78
	EAP_s	42.99	38.82	1.21	0	52.19	-0.79	-1.42	-0.48	41.38	-9.91
	EAP_i	-12.53	-19.84	-52.22	-52.19	0	-57.37	-52.43	-52.63	-13.82	-58.96
	EMAP	42.73	38.90	2.53	0.79	57.37	0	-0.65	0.35	44.51	-10.37
Proposed attributes	$EAPPR_a$	43.28	40.15	3.98	1.42	52.43	0.65	0	1.02	42.10	-8.37
	$EAPPR_s$	42.92	38.47	1.56	0.48	52.63	-0.35	-1.02	0	42.28	-9.42
	$EAPPR_i$	0.58	-5.97	-40.60	-41.38	13.82	-44.51	-42.10	-42.28	0	-51.24
	EMAPPR	47.91	44.24	10.78	9.91	58.96	10.37	8.37	9.42	51.24	0

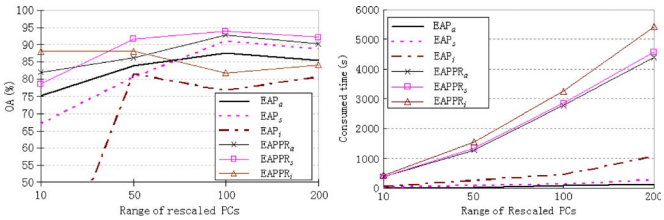

(a) (b)

Fig. 14. Classification accuracy and consumed time with different ranges of rescaled PCs to generate single APs. (a) Overall classification accuracy. (b) Consumed time.

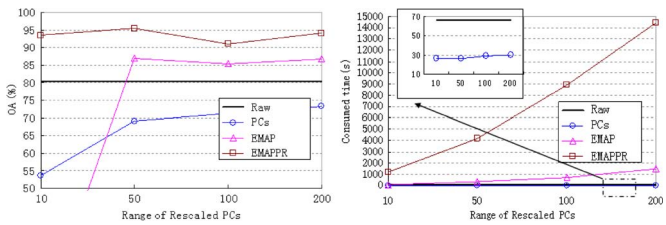

(a) (b)

Fig. 15. Classification accuracy and consumed time with different ranges of rescaled PCs to generate EAPs. (a) Overall classification accuracy. (b) Consumed time.

E. Results on Rescaling PCs Into Different Ranges

In this experiment, we take *University Area* as an example to investigate the robustness of the existing APs and our proposed APs with partial reconstruction to the ranges of the rescaled PCs.

We first rescale the selected PCs to different ranges (e.g., [0, 10], [0, 50], [0, 100], and [0, 200]) and convert them into gray-level image according to the corresponding ranges before applying AFs. In order to compute different attributes on the rescaled PCs, we keep the values of "area" and "MI" fixed: $\lambda_a = [100, 500, 1000, 2000, 3000, 4000, 5000]$ and $\lambda_i = [0.15, 0.2, 0.25, 0.3, 0.35, 0.4, 0.45]$. The values of the "Std" attribute are changed according to the gray level of rescaled PCs: $\lambda_s = [0.05, 0.1, 0.2, 0.3, 0.4, 0.5, 0.6]$ for the PCs rescaled into range [0, 10], $\lambda_s = [0.25, 0.5, 1, 1.5, 2, 2.5, 3]$ for range [0, 50], and $\lambda_s = [0.5, 1, 2, 3, 4, 5, 6]$ for range [0, 100].

TABLE V
University Houston: CLASSIFICATION ACCURACIES OBTAINED BY ORIGINAL APS AND OUR PROPOSED APS WITH PARTIAL RECONSTRUCTION. THE FIRST TWO PCS ARE ALL RESCALED INTO RANGE [0, 100]

	Raw	PCs	Original attribute profiles				Proposed attribute profiles			
			EAP_a	EAP_s	EAP_i	EMAP	$EAPPR_a$	$EAPPR_s$	$EAPPR_i$	EMAPPR
No. Fea	144	2	30	30	30	90	30	30	30	90
OA	92.65	80.02	91.90	90.87	86.45	93.01	93.39	92.47	89.27	**95.29**
AA	93.04	80.63	92.54	91.39	88.21	93.81	93.91	93.22	90.05	**95.47**
κ	0.920	0.784	0.912	0.901	0.854	0.924	0.928	0.919	0.884	**0.949**
(#198 / #875) Grass Healthy	**99.16**	**99.16**	98.32	97.76	98.42	98.79	98.51	97.30	96.18	98.88
(#154 / #856) Grass Stressed	96.14	94.75	95.15	96.14	98.02	96.83	**99.21**	98.02	99.11	98.51
(#192 / #505) Grass Synthetis	**100.0**	93.11	**100.0**	**100.0**	**100.0**	99.71	**100.0**	**100.0**	**100.0**	99.71
(#173 / #880) Tree	99.43	97.34	98.20	97.91	95.54	96.96	**99.53**	98.67	96.39	94.68
(#186 / #1056) Soil	98.47	97.18	99.60	97.18	95.01	93.64	99.52	99.36	96.54	**99.92**
(#182 / #143) Water	97.85	94.46	97.23	**99.69**	**99.69**	**99.69**	97.85	97.85	**99.69**	98.15
(#183 / #795) Residential	**89.67**	53.99	92.74	83.03	77.71	86.61	87.42	88.75	87.63	87.12
(#158 / #494) Commercial	73.93	38.34	75.31	67.02	69.02	**84.05**	80.98	72.24	67.18	82.98
(#149 / #891) Road	81.54	78.17	85.19	90.38	76.25	**92.31**	81.35	87.31	72.02	89.62
(#109 / #299) Highway	98.04	97.55	**100.0**	**100.0**	99.02	**100.0**	**100.0**	**100.0**	98.77	**100.0**
(#110 / #426) Railway	95.15	83.40	92.91	96.83	91.42	94.03	97.39	**99.81**	88.43	99.07
(#192 / #1041) Parking Lot 1	82.73	42.58	71.61	73.24	51.09	79.81	82.97	74.37	73.56	**95.05**
(#184 / #265) Parking Lot 2	84.86	44.10	83.07	72.16	75.50	85.30	83.96	84.63	78.17	**88.42**
(#181 / #247) Tennis Court	99.77	98.13	98.83	99.53	98.60	99.53	**100.0**	**100.0**	98.60	**100.0**
(#187 / #473) Running Track	98.94	97.12	**100.0**	**100.0**	97.88	99.85	**100.0**	**100.0**	98.48	**100.0**

TABLE VI
UNIVERSITY HOUSTON: STATISTICAL SIGNIFICANCE OF DIFFERENCES IN CLASSIFICATION (Z) WHEN THE FIRST FEW PCS ARE RESCALED INTO RANGE [0, 100]. EACH CASE OF THE TABLE REPRESENTS Z_{rc} WHERE r IS THE ROW AND c IS THE COLUMN

Z_{rc}		Raw	PCs	Original attributes				Proposed attributes			
				EAP_a	EAP_s	EAP_i	EMAP	$EAPPR_a$	$EAPPR_s$	$EAPPR_i$	EMAPPR
Raw		0	33.45	2.72	6.16	20.25	-1.23	-2.8	0.69	11.38	-9.90
PCs		-33.45	0	-33.86	-30.36	-17.79	-34.14	-35.63	-33.01	-24.70	-37.44
Original attributes	EAP_a	-2.72	33.86	0	4.46	19.34	-5.22	-6.48	-2.23	9.30	-12.82
	EAP_s	-6.16	30.36	-4.46	0	14.64	-8.64	-9.96	-6.43	5.37	-16.15
	EAP_i	-20.25	17.79	-19.34	-14.46	0	-22.49	-22.90	-20.24	-9.33	-27.25
	EMAP	1.23	34.14	5.22	8.64	22.49	0	-1.61	2.13	12.49	-9.52
Proposed attributes	$EAPPR_a$	2.8	35.63	6.48	9.96	22.90	1.61	0	4.33	14.43	-7.82
	$EAPPR_s$	-0.69	33.01	2.23	6.43	20.24	-2.13	-4.33	0	10.99	-10.89
	$EAPPR_i$	-11.38	24.70	-9.3	-5.37	9.33	-12.49	-14.43	-10.99	0	-20.99
	EMAPPR	9.90	37.44	12.82	16.15	27.25	9.52	7.82	10.89	20.99	0

Fig. 14 shows the OA and consumed time to generate each individual EAPs and EAPPRs with different ranges of rescaled PCs. Fig. 15 shows the relationship of OA by stacking all EAPs/EAPPRs (i.e., EMAPs/EMAPPRs) and total consumed time of generated EMAPs/EMAPPRs with different ranges of rescaled PCs. We take a very low range as an example to see the effects of connecting objects in classification for a remote sensed image. The resulting accuracies are reported in Table VII, and the classification maps are shown in Fig. 16.

From the tables and figure, we can make the following remarks.

1) By using morphological thinning/thickening with partial reconstruction to separate connected objects in each gray level, our proposed attribute thinning and thickening take much more time to compute the APs but enable better performances on classification. The consumed time depends on the range of rescaled PCs; the bigger the range is, the more consumed time it takes. The attribute of "MI" consumes more time than other attributes. For example, with PCs rescaled in the lower range [0, 10], the original AFs consume 9.82, 15.68, and 52.21 s to generate the attributes of "area," "Std," and "MI," respectively, while the proposed AFs with partial reconstruction require 383.29, 389.04, and 440.49 s for the attributes of "area," "Std," and "MI," respectively. With morphological partial reconstruction, the proposed AFs increase the processing time to generate different APs, by eight times more than the original AFs. We do benefit much better performances for classification with partial reconstruction. The classification by using EAP_i is really worse, and many classes are misclassified as "Soil," with very low OA (11.76%). The proposed $EAPPR_i$ produces much better results than other attributes, with 77% OA improvements over EAP_i and 7%–20% OA improvements over other attributes. Moreover, our proposed EMAPPR can get much better results with PCs rescaled in such a lower range than that EMAP built on PCs rescaled to range [0, 200] and [0, 1000], with less processing time.
2) The proposed APs with partial reconstruction are more robust to the ranges of rescaled PCs. The performances of classification by using our proposed EMAPPR are more stable, even with PCs rescaling to a very low range (e.g., [0, 10]), where the original EMAP performs very worse.
3) Many objects are connected when the selected PCs are rescaled into a very low range (e.g., [0, 10]; see Fig. 8), which leads to very poor classification performance [see Fig. 16(a)]. Although the classification map looks smoother, many objects are misclassified by using the original EMAP because many objects are connected, particularly for class "Gravel," with less 10% accuracies by

TABLE VII
University Area: CLASSIFICATION ACCURACIES OBTAINED BY ORIGINAL APS AND OUR PROPOSED APS WITH PARTIAL RECONSTRUCTION. THE FIRST FOUR PCS ARE ALL RESCALED INTO RANGE [0, 10]

	PCs	Original attribute profiles				Proposed attribute profiles			
		EAP_a	EAP_s	EAP_i	EMAP	$EAPPR_a$	$EAPPR_s$	$EAPPR_i$	EMAPPR
No. Fea	4	36	36	36	108	36	36	36	108
OA	53.78	75.20	67.20	11.76	11.76	81.95	78.19	88.14	**93.49**
AA	68.05	78.78	75.67	11.11	11.11	89.57	78.93	85.87	**93.69**
κ	44.26	68.09	59.35	0	0	76.81	71.44	84.05	**91.24**
Asphalt	43.78	82.66	81.60	0	0	**95.46**	83.94	95.43	95.05
Meadows	42.04	72.56	54.84	0	0	74.16	82.80	95.81	**98.24**
Gravel	5.10	7.00	1.43	0	0	93.62	49.31	58.17	**95.24**
Trees	**96.51**	90.70	95.07	0	0	94.06	85.25	77.42	93.60
Metal Sheets	98.59	99.26	99.26	0	0	**100**	**100**	99.93	**100**
Soil	44.58	59.63	62.70	**100**	**100**	66.71	61.68	62.28	66.06
Bitumen	87.82	**99.92**	91.88	0	0	99.47	87.82	98.80	99.02
Bricks	96.01	**98.64**	95.63	0	0	83.92	60.84	86.72	97.31
Shadows	97.99	98.63	98.63	0	0	**98.73**	**98.73**	98.31	**98.73**

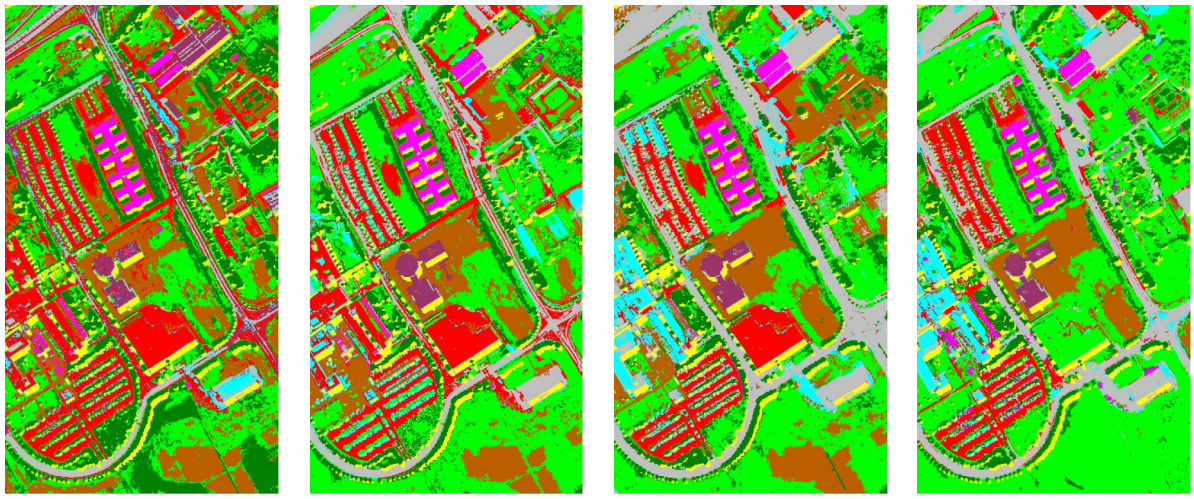

(a) (b) (c) (d)

Fig. 16. Classification maps for *University Area* when the first four PCs are rescaled into range [0, 10]. (a) Rescaled PCs, (b) EAP_a, (c) proposed $EAPPR_a$, and (d) proposed EMAPPR.

using the original "area" and "Std" attributes, because it is misclassified into its bigger connected object "Asphalt."

4) When using the existing attribute thinning and thickening, it is better sometimes to use single EAPs than simply stacking many of them for classification. The original EMAP produces much worse results than only using single EAPs built with "area" and "Std" attributes. For each single AP, the EAPPRs constructed by using the proposed attribute thinning and thickening with partial reconstruction perform better than EAPs constructed by the existing attribute thinning and thickening. The improvements of our proposed EAPPRs over EAPs are almost 6.75%, 10.99%, and 76.38% for area, Std, and MI attributes, respectively. Moreover, when stacking all single EAPPRs generated by our proposed method, it enables better performances on classification.

In many real applications, the users want to get a classification map with satisfying accuracies and without waiting too long. They may not have enough backgrounds on parameter optimizing (e.g., which ranges will be good for rescaling the selected PCs, the size of the objects in an image, etc.). They always select all these parameters randomly. The original attribute opening and closing are not robust to the ranges of the rescaled PCs. This is because more and more objects are connected when the selected PCs are converted into gray-level images with a lower range. The attributes of an object will mix with its largest connected object, which will lead to poor classification performances.

The APs generated by our proposed attribute thinning and thickening with partial reconstruction better model the spatial information of objects in an image. Our approach is more robust to the ranges of rescaled PCs as it can separate connected objects. Moreover, our proposed APs with partial reconstruction contain less redundant information because connected objects will disappear according to their scales. This makes our proposed method more robust on selecting values for different attributes and enables better performances when stacking each single attribute together.

VI. CONCLUSION

In this paper, we have developed a novel framework for attribute thinning and thickening with partial reconstruction. A main contribution of the presented approach is that it can separate connected objects and thus better models the spatial

information of objects in an image. Our main goal is to address a common situation in the existing attribute thinning and thickening by reconstruction, in which the attributes of the connected objects in an image are not well modeled. Objects expected to disappear at a certain threshold remain present when they are connected with other objects in the image. The attributes of small objects are mixed with their larger connected objects, which leads to poor performances on classification. Morphological APs have been widely used in many applications and improved the performances of classification compared to only using spectral information. However, in many real applications, the users may not have enough backgrounds on parameter optimizing (e.g., which ranges will be good for rescaling the selected features, how to select the values of different attributes, etc.). They always select all these parameters randomly. The existing attribute thinning and thickening are not robust to the ranges of the rescaled PCs. This is because more and more objects are connected when the selected features (e.g., the first few PCs) are converted into gray-level images with a lower range. Moreover, the EAPs generated by using the existing attribute thinning and thickening by reconstruction contain redundant information because objects will survive in many scales if connected with larger objects.

The experiments on a variety of hyperspectral scenes confirmed expected improvements of our approach over the existing attribute thinning and thickening by reconstruction. The improvements become more significant when more objects from different classes are connected (e.g., the selected features are converted to a lower rescaled range) or when stacking all single attributes together. The proposed approach better models the spatial information of objects in an image and thus enables better performances on classification. In addition, the proposed approach is very robust to the ranges of rescaled features; it can separate connected objects and enable good classification performances even when the selected features are rescaled into a very low range, where EAPs generated by the existing attribute thinning and thickening perform worse. Last but not least, the EAPs generated by our proposed approach contain less redundant information, which makes our proposed method more robust on selecting values for different attributes and enables better performances when stacking all single attributes together.

Our future work will include, but will not be limited to, the following topics.

1) Data fusion of multiple features generated by the proposed thinning and thickening with partial reconstruction. Recent work on multiple feature learning [16] and graph fusion [37] shows the efficiency of fusion multiple features (e.g., MPs and EAPs) for classification. Some recent methods on advanced classifiers (e.g., rotation forest [38] and random subspace ensembles [39]) and automatic threshold selection [40] for APs will be exploited.
2) Exploitation of high-level features by using the proposed thinning and thickening with partial reconstruction to construct some information indexes, such as morphological building/shadow index [41], which has been proven efficiently for the classification and change detection of high-resolution remotely sensed images over urban areas [42], [43].
3) Developing parallel versions of the proposed framework in a variety of architectures, such as commodity graphics processing units (GPUs) or multi-GPU platforms.

ACKNOWLEDGMENT

The authors would like to thank Prof. P. Gamba from the University of Pavia, Italy, for kindly providing both the *Pavia Center* and *Pavia University* data sets, the Hyperspectral Image Analysis group, and the NSF-Funded Center for Airborne Laser Mapping at the University of Houston for providing the *Houston University* hyperspectral image.

REFERENCES

[1] M. Pesaresi and J. A. Benediktsson, "A new approach for the morphological segmentation of high-resolution satellite imagery," *IEEE Trans. Geosci. Remote Sens.*, vol. 39, no. 2, pp. 309–320, Feb. 2001.
[2] J. A. Benediktsson, J. Palmason, and J. R. Sveinsson, "Classification of hyperspectral data from urban areas based on extended morphological profiles," *IEEE Trans. Geosci. Remote Sens.*, vol. 43, no. 3, pp. 480–491, Mar. 2005.
[3] P. Soille, *Morphological Image Analysis, Principles and Applications*, 2nd ed. Berlin, Germany: IEEE, 2003.
[4] A. Plaza, P. Martinez, J. Plaza, and R. M. Perez, "Dimensionality reduction and classification of hyperspectral image data using sequences of extended morphological transformations," *IEEE Trans. Geosci. Remote Sens.*, vol. 43, no. 3, pp. 466–479, Mar. 2005.
[5] M. Fauvel, J. Chanussot, and J. A. Benediktsson, "Kernel principal component analysis for the classification of hyperspectral remote-sensing data over urban areas," *EURASIP J. Adv. Signal Process.*, vol. 2009, Feb. 2009, Art. ID 783194.
[6] L. Vincent, "Morphological grayscale reconstruction: Definition, efficient algorithm and applications in image analysis," in *Proc. IEEE Conf. Comput. Vis. Pattern Recognit.*, Champaign, IL, USA, Jun. 1992, pp. 633–635.
[7] L. Vincent, "Morphological grayscale reconstruction in image analysis: Applications and efficient algorithms," *IEEE Trans. Image Process.*, vol. 2, no. 2, pp. 176–201, Feb. 1993.
[8] R. Bellens *et al.*, "Improved classification of VHR images of urban areas using directional morphological profiles," *IEEE Trans. Geosci. Remote Sens.*, vol. 46, no. 10, pp. 2803–2812, Oct. 2008.
[9] M. Dalla Mura, J. A. Benediktsson, B. Waske, and L. Bruzzone, "Morphological attribute profiles for the analysis of very high resolution images," *IEEE Trans. Geosci. Remote Sens.*, vol. 48, no. 10, pp. 3747–3762, Oct. 2010.
[10] M. Dalla Mura, J. A. Benediktsson, B. Waske, and L. Bruzzone, "Extended profiles with morphological attribute filters for the analysis of hyperspectral data," *Int. J. Remote Sens.*, vol. 31, no. 22, pp. 5975–5991, Nov. 2010.
[11] M. Dalla Mura, A. Villa, J. A. Benediktsson, J. Chanussot, and L. Bruzzone, "Classification of hyperspectral images by using extended morphological attribute profiles and independent component analysis," *IEEE Geosci. Remote Sens. Lett.*, vol. 8, no. 3, pp. 541–545, May 2011.
[12] M. Pedergnana, P. Reddy Marpu, M. Dalla Mura, J. A. Benediktsson, and L. Bruzzone, "Classification of remote sensing optical and LiDAR data using extended attribute profiles," *IEEE J. Sel. Topics Signal Process.*, vol. 6, no. 7, pp. 856–865, Nov. 2012.
[13] M. Pedergnana, P. R. Marpu, M. Dalla Mura, J. A. Benediktsson, and L. Bruzzone, "A novel technique for optimal feature selection in attribute profiles based on genetic algorithms," *IEEE Trans. Geosci. Remote Sens.*, vol. 51, no. 6, pp. 3514–3528, Jun. 2013.
[14] P. Ghamisi, J. A. Benediktsson, and J. R. Sveinsson, "Automatic spectral-spatial classification framework based on attribute profiles and supervised feature extraction," *IEEE Trans. Geosci. Remote Sens.*, vol. 52, no. 9, pp. 5771–5782, May 2014.
[15] B. Song *et al.*, "Remotely sensed image classification using sparse representations of morphological attribute profiles," *IEEE Trans. Geosci. Remote Sens.*, vol. 52, no. 8, pp. 5122–5136, Aug. 2014.
[16] J. Li *et al.*, "Multiple feature learning for hyperspectral image classification," *IEEE Trans. Geosci. Remote Sens.*, vol. 53, no. 3, pp. 1592–1606, Mar. 2015.

[17] P. Salembier and M. Wilkinson, "Connected operators: A review of region-based morphological image processing techniques," *IEEE Signal Process. Mag.*, vol. 26, no. 6, pp. 136–157, Nov. 2009.
[18] G. K. Ouzounis and M. H. F. Wilkinson, "Mask-based second generation connectivity and attribute filters," *IEEE Trans. Pattern Anal. Mach. Intell.*, vol. 29, no. 6, pp. 990–1004, Jun. 2007.
[19] M. H. F. Wilkinson, "Connected filtering by reconstruction: Basis and new advances," in *Proc. IEEE 15th ICIP*, Oct. 2008, pp. 2180–2183.
[20] G. K. Ouzounis and M. H. F. Wilkinson, "Partition-induced connections and operators for pattern analysis," *Pattern Recognit.*, vol. 43, no. 10, pp. 3193–3207, Oct. 2010.
[21] T. Castaings, B. Waske, J. A. Benediktsson, and J. Chanussot, "On the influence of feature reduction for the classification of hyperspectral images based on the extended morphological profile," *Int. J. Remote Sens.*, vol. 31, no. 22, pp. 5921–5939, Jul. 2010.
[22] W. Liao, R. Bellens, A. Pižurica, W. Philips, and Y. Pi, "Classification of hyperspectral data over urban areas using directional morphological profiles and semi-supervised feature extraction," *IEEE J. Sel. Topics Appl. Earth Observ. Remote Sens.*, vol. 5, no. 4, pp. 1177–1190, Aug. 2012.
[23] W. Liao, R. Bellens, A. Pižurica, W. Philips, and Y. Pi, "Classification of hyperspectral data over urban areas based on extended morphological profile with partial reconstruction," in *Proc. ACIVS*, Brno, Czech Republic, 2012, pp. 278–289.
[24] C. Debes *et al.*, "Hyperspectral and LiDAR data fusion: Outcome of the 2013 GRSS data fusion contest," *IEEE J. Sel. Topics Appl. Earth Observ. Remote Sens.*, vol. 7, no. 6, pp. 2405–2418, Jun. 2014.
[25] W. Liao, R. Bellens, A. Pizurica, S. Gautama, and W. Philips, "Generalized graph-based fusion of hyperspectral and LiDAR data using morphological features," *IEEE Geosci. Remote Sens. Lett.*, vol. 12, no. 3, pp. 552–556, Mar. 2015.
[26] Z. Mahmood, G. Thoonen, and P. Scheunders, "Automatic threshold selection for morphological attribute profiles," in *Proc. IEEE IGARSS*, Munich, Germany, Jul. 22–27, 2012, pp. 4946–4949.
[27] J. Crespo, J. Serra, and R. Shafer, "Theoretical aspects of morphological filters by reconstruction," *Signal Process.*, vol. 47, no. 2, pp. 201–225, Nov. 1995.
[28] M. Fauvel, J. A. Benediktsson, J. Chanussot, and J. R. Sveinsson, "Spectral and spatial classification of hyperspectral data using SVMs and morphological profile," *IEEE Trans. Geosci. Remote Sens.*, vol. 46, no. 11, pp. 3804–3814, Nov. 2008.
[29] E. J. Breen and R. Jones, "Attribute openings, thinnings and granulometries," *Comput. Vis. Image Understand.*, vol. 64, no. 3, pp. 377–389, Nov. 1996.
[30] P. Salembier and M. H. F. Wilkinson, "Connected operators," *IEEE Signal Process. Mag.*, vol. 26, no. 6, pp. 136–157, Nov. 2009.
[31] Hyperspectral Remote Sensing Scenes. [Online]. Available: http://www.ehu.eus/ccwintco/index.php?title=Hyperspectral_Remote_Sensing_Scenes/
[32] 2013 IEEE GRSS Data Fusion Contest. [Online]. Available: http://www.grss-ieee.org/community/technical-committees/data-fusion/
[33] C. J. C. Burges, "A tutorial on support vector machines for pattern recognition," *Data Mining Knowl. Discovery*, vol. 2, no. 2, pp. 121–167, Jun. 1998.
[34] C. C. Chang and C. J. Lin, "LIBSVM: A library for support vector machines," *ACM Trans. Intell. Syst. Technol.*, vol. 2, no. 3, pp. 1–27, Apr. 2011.
[35] G. F. Hughes, "On the mean accuracy of statistical pattern recognizers," *IEEE Trans. Inf. Theory*, vol. 14, no. 1, pp. 55–63, Jan. 1968.
[36] G. M. Foody, "Thematic map comparison: Evaluating the statistical significance of differences in classification accuracy," *Photogramm. Eng. Remote Sens.*, vol. 70, no. 5, pp. 627–633, May 2004.
[37] W. Liao *et al.*, "Processing of multiresolution thermal hyperspectral and digital color data: Outcome of the 2014 IEEE GRSS data fusion contest," *IEEE J. Sel. Topics Appl. Earth Observ. Remote Sens.*, vol. 8, no. 6, pp. 2984–2996, May 2015.
[38] J. Xia, P. Du, X. He, and J. Chanussot, "Hyperspectral remote sensing image classification based on rotation forest," *IEEE Geosci. Remote Sens. Lett.*, vol. 11, no. 1, pp. 239–243, Jan. 2014.
[39] J. Xia, M. Dalla Mura, J. Chanussot, P. Du, and X. He, "Random subspace ensembles for hyperspectral image classification with extended morphological attribute profiles," *IEEE Trans. Geosci. Remote Sens.*, vol. 53, no. 9, pp. 4768–4786, Mar. 2015.
[40] G. Cavallaro, N. Falco, M. Dalla Mura, L. Bruzzone, and J. A. Benediktsson, "Automatic threshold selection for profiles of attribute filters based on granulometric characteristic functions," in *Proc. 12th Int. Symp. ISMM*, Reykjavik, Iceland, 2015, vol. 9082, pp. 169–181.
[41] X. Huang and L. Zhang, "Morphological building/shadow index for building extraction from high-resolution imagery over urban areas," *IEEE J. Sel. Topics Appl. Earth Observ. Remote Sens.*, vol. 5, no. 1, pp. 161–172, Feb. 2012.
[42] X. Huang, Q. Lu, and L. Zhang, "A multi-index learning approach for classification of high-resolution remotely sensed images over urban areas," *ISPRS J. Photogramm. Remote Sens.*, vol. 90, pp. 36–48, Apr. 2014.
[43] X. Huang, H. Liu, and L. Zhang, "Spatiotemporal detection and analysis of urban villages in mega city regions of China using high-resolution remotely sensed imagery," *IEEE Trans. Geosci. Remote Sens.*, vol. 53, no. 7, pp. 3639–3657, Jan. 2015.

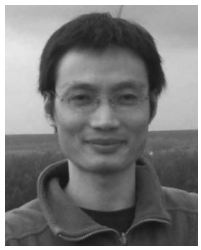

Wenzhi Liao (M'14) received the B.S. degree in mathematics from Hainan Normal University, Haikou, China, in 2006, the Ph.D. degree in engineering from South China University of Technology, Guangzhou, China, in 2012, and the Ph.D. degree in computer science engineering from Ghent University, Ghent, Belgium, in 2012.

Since 2012, he has worked as a Postdoctoral Researcher at Ghent University. His current research interests include pattern recognition, remote sensing, and image processing. In particular, his interests include mathematical morphology, multitask feature learning, multisensor data fusion, and hyperspectral image restoration.

Dr. Liao is a member of the Geoscience and Remote Sensing Society (GRSS) and IEEE GRSS Data Fusion Technical Committee. He was the recipient of the "Best Paper Challenge" Awards on both the 2013 IEEE GRSS Data Fusion Contest and the 2014 IEEE GRSS Data Fusion Contest.

Mauro Dalla Mura (S'08–M'11) received the laurea (B.E.) and laurea specialistica (M.E.) degrees in telecommunication engineering from the University of Trento, Trento, Italy, in 2005 and 2007, respectively. He obtained in 2011 a joint Ph.D. degree in information and communication technologies (telecommunications area) from the University of Trento and in electrical and computer engineering from the University of Iceland, Reykjavík, Iceland.

In 2011, he was a Research Fellow at Fondazione Bruno Kessler, Trento, Italy, conducting research on computer vision. He is currently an Assistant Professor at the Grenoble Institute of Technology (Grenoble INP), Grenoble, France. He is conducting his research at the Grenoble Images Speech Signals and Automatics Laboratory (GIPSA-Lab). His main research activities are in the fields of remote sensing, image processing, and pattern recognition. In particular, his interests include mathematical morphology, classification, and multivariate data analysis.

Dr. Dalla Mura is a Reviewer of the IEEE TRANSACTIONS ON GEOSCIENCE AND REMOTE SENSING, IEEE GEOSCIENCE AND REMOTE SENSING LETTERS, IEEE JOURNAL OF SELECTED TOPICS IN EARTH OBSERVATIONS AND REMOTE SENSING, IEEE JOURNAL OF SELECTED TOPICS IN SIGNAL PROCESSING, *Pattern Recognition Letters*, *International Society for Photogrammetry and Remote Sensing (ISPRS) Journal of Photogrammetry and Remote Sensing*, and *Photogrammetric Engineering and Remote Sensing*. He is a member of the Geoscience and Remote Sensing Society (GRSS) and IEEE GRSS Data Fusion Technical Committee and the Secretary of the IEEE GRSS French Chapter (2013–2016). He was a Lecturer at the RSSS12-Remote Sensing Summer School 2012 (organized by the IEEE GRSS), Munich, Germany. He was the recipient of the IEEE GRSS Second Prize in the Student Paper Competition of the 2011 IEEE International Geoscience and Remote Sensing Symposium (IGARSS) 2011 and a corecipient of the Best Paper Award of the International Journal of Image and Data Fusion for the year 2012–2013 and the Symposium Paper Award for IEEE IGARSS 2014.

Jocelyn Chanussot (M'04–SM'04–F'12) received the M.Sc. degree in electrical engineering from the Grenoble Institute of Technology (Grenoble INP), Grenoble, France, in 1995, and the Ph.D. degree from Savoie University, Annecy, France, in 1998.

In 1999, he was with the Geography Imagery Perception Laboratory for the Delegation Generale de l'Armement (DGA-French National Defense Department). Since 1999, he has been with Grenoble INP, where he was an Assistant Professor from 1999 to 2005 and an Associate Professor from 2005 to 2007 and is currently a Professor of signal and image processing. He is conducting his research at the Grenoble Images Speech Signals and Automatics Laboratory (GIPSA-Lab). His research interests include image analysis, multicomponent image processing, nonlinear filtering, and data fusion in remote sensing. He has been a Visiting Scholar at Stanford University, Stanford, California (USA), The Royal Institute of Technology (Sweden), and National University of Singapore (Singapore). Since 2013, he has been an Adjunct Professor of the University of Iceland. He has supervised Ph.D. students from ten different countries (Brazil, China, Egypt, France, Italy, Montenegro, Pakistan, Portugal, Ukraine, and Spain).

Dr. Chanussot is the founding President of the IEEE Geoscience and Remote Sensing French Chapter (2007–2010) which received the 2010 IEEE Geoscience and Remote Sensing Society (GRS-S) Chapter Excellence Award. He was a corecipient of the NORSIG 2006 Best Student Paper Award, the IEEE GRSS 2011 Symposium Best Paper Award, the IEEE GRSS 2012 Transactions Prize Paper Award, and the IEEE GRSS 2013 Highest Impact Paper Award. He was a member of the IEEE Geoscience and Remote Sensing Society Administrative Committee (2009–2010), in charge of membership development. He was the General Chair of the first IEEE GRSS Workshop on Hyperspectral Image and Signal Processing, Evolution in Remote sensing (WHISPERS). He was the Chair (2009–2011) and Cochair of the Geoscience and Remote Sensing Society (GRS) Data Fusion Technical Committee (2005–2008). He was a member of the Machine Learning for Signal Processing Technical Committee of the IEEE Signal Processing Society (2006–2008) and the Program Chair of the IEEE International Workshop on Machine Learning for Signal Processing (2009). He was an Associate Editor for the IEEE GEOSCIENCE AND REMOTE SENSING LETTERS (2005–2007) and for Pattern Recognition (2006–2008). Since 2007, he has been an Associate Editor for the IEEE TRANSACTIONS ON GEOSCIENCE AND REMOTE SENSING. Since 2011, he has been the Editor-in-Chief of the IEEE JOURNAL OF SELECTED TOPICS IN APPLIED EARTH OBSERVATIONS AND REMOTE SENSING. He was a Guest Editor for the PROCEEDINGS OF THE IEEE in 2013 and a Guest Editor for the IEEE SIGNAL PROCESSING MAGAZINE in 2014. He is a member of the Institut Universitaire de France (2012–2017).

Rik Bellens (M'07) received the diploma in computer science engineering from Ghent University, Ghent, Belgium, in 2004, where he is currently working toward the Ph.D. degree in the Department of Telecommunications and Information Processing.

His main research interests are pattern recognition, remote sensing, image processing, mobility, and crowd behavior.

Wilfried Philips (S'90–M'93–SM'10) was born in Aalst, Belgium, on October 19, 1966. He received the Diploma degree in electrical engineering and the Ph.D. degree in applied sciences from Ghent University, Ghent, Belgium, in 1989 and 1993, respectively.

From October 1989 to October 1997, he worked with the Department of Electronics and Information Systems, Ghent University, for the Flemish Fund for Scientific Research (FWO-Vlaanderen), first as a Research Assistant and later as a Postdoctoral Research Fellow. Since November 1997, he has been with the Department of Telecommunications and Information Processing, Ghent University, where he is currently a Full-Time Professor and is the Head of the research group "Image Processing and Interpretation," which is part of the virtual Flemish Information and Communication Technology (ICT) Research Institute iMinds. His research interests include image and video restoration, analysis and modeling of image reproduction systems, remote sensing, surveillance, and industrial inspection.